FISEVIER

Contents lists available at ScienceDirect

## International Immunopharmacology

journal homepage: www.elsevier.com/locate/intimp





# Human umbilical cord mesenchymal stem cell-derived exosomes loaded miR-451a targets ATF2 to improve rheumatoid arthritis

Liangyu Mi $^{a,b,1}$ , Jinfang Gao $^{b,1}$ , Na Li $^{a,c,1}$ , Ying Liu $^b$ , Na Zhang $^b$ , Yanan Gao $^{a,b}$ , Xinyue Peng $^{a,b}$ , Liyun Zhang $^b$ , Ke Xu $^{b,*}$ 

- a Third Hospital of Shanxi Medical University, Shanxi Bethune Hospital, Shanxi Academy of Medical Sciences, Tongji Shanxi Hospital, Taiyuan, China
- b Department of Rheumatology, Shanxi Bethune Hospital, Shanxi Academy of Medical Sciences, Tongji Shanxi Hospital, Third Hospital of Shanxi Medical University, Taiyuan, China
- <sup>c</sup> Shanxi Medical University School and Hospital of Stomatology, Taiyuan, China

#### ARTICLE INFO

#### Keywords: Rheumatoid arthritis Synovial fibroblasts Mesenchymal stem cells Exosomes miRNA-451a

#### ABSTRACT

Objective: Rheumatoid arthritis (RA) is an autoimmune disease characterized by chronic joint inflammation, with synovial fibroblasts (SFs) playing a pivotal role in its pathogenesis. Dysregulation of microRNA (miRNA) expression in SFs contributes to RA development. Exosomes (Exos) have emerged as effective carriers for therapeutic molecules, facilitating miRNA transfer between cells. This study explores the therapeutic potential of Exos derived from human umbilical cord mesenchymal stem cells (hUCMSCs), loaded with miR-451a, to modulate ATF2 expression, aiming to address RA in both in vivo and in vitro settings.

Methods: In this study, hUCMSC and RA SFs were isolated and identified, and hUCMSC-Exos were extracted and characterized. The influence of hUCMSC-Exos on RA SFs was detected. And hUCMSC-Exos targeting RA SFs was traced. HUCMSC<sup>KD-AGO2</sup> was prepared by knocking down AGO2 in hUCMSC. HUCMSC<sup>KD-AGO2</sup>-Exos was extracted and characterized, and their influence on RA SFs was detected. The miRNA profiles before and after hUCMSC-Exos intervention in RA SFs were mapped to identify differential miRNAs. RT-qPCR was used to verify the differential miRNAs, with hsa-miR-451a finally selected as the target gene. The effect of miR-451a on SFs was detected. The latent binding of miR-451a to activating transcription factor 2 (ATF2) was analyzed. The effect of hUCMSC-Exos<sup>miR-451a</sup> on SFs was detected, and the expression of miR-451a and ATF2 was measured by RT-PCR. In vivo, hUCMSC-Exos<sup>miR-451a</sup> was injected into the ankle joint of CIA rats, and arthritis index, joint imaging and synovial pathology were assessed. The expression of miR-451a and ATF2 in synovial tissue was detected. Finally, the safety of hUCMSC-Exos<sup>miR-451a</sup> in CIA rats was evaluated.

Results: This study revealed that hUCMSC-Exos can inhibit RA SFs proliferation, migration and invasion through miRNAs. High throughput sequencing detected 13 miRNAs that could be transmitted from hUCMSCs to RA SFs via hUCMSC-Exos. miR-451a inhibited RA SFs proliferation, migration and invasion by regulating ATF2. hUCMSC-Exos loaded with miR-451a targeted ATF2 to inhibit RA SFs proliferation, migration and invasion, and improve joint inflammation and imaging findings in CIA rats.

Conclusions: This study demonstrates that miR-451a carried by hUCMSC-Exos can play a role in inhibiting RA SFs biological traits and improving arthritis in CIA rats by inhibiting ATF2. The findings suggest a promising treatment for RA and provide insights into the mechanism of action of hUCMSC-Exos in RA. Future research directions will continue to explore the potential in this field.

### 1. Introduction

Rheumatoid arthritis (RA) is an autoimmune disease characterized by chronic synovial proliferation and progressive joint destruction. The typical pathological changes of RA are abnormal synovial hyperplasia and destruction of cartilage and bone. Synovial fibroblasts (SFs) in RA patients play a central role in the formation and chronicization of RA joint inflammation and cartilage degradation [1]. RA SFs have been in a

https://doi.org/10.1016/j.intimp.2023.111365

 $<sup>^{\</sup>star}$  Corresponding author.

E-mail address: xukesxbqeh@hotmail.com (K. Xu).

 $<sup>^{1}</sup>$  Liangyu Mi, Jinfang Gao and Na Li contributed equally to this work.

state of chronic activation, and obstacles to the growth regulatory mechanism lead to "tumor-like growth" of cells, excessive proliferation, inhibition of apoptosis, and aggressiveness. At the same time, RA SFs migrate and produce matrix degrading enzymes, such as matrix metalloproteinases (MMPs) and cathepsin. These enzymes secrete a series of inflammatory factors such as tumor necrosis factor-α (TNF-α), interleukin (IL) -1\beta, IL-6, and chemokines Interferon-induced protein 10, stromal cell-derived factor-1, monocyte chemoattraetant protein-1 [2,3], and cause chronic persistent arthritis. Receptor activator of nuclear factor kappa-B ligand (RANKL) binds to receptor activator of nuclear factor kappa-B on osteoclast precursor cells to directly induce bone destruction. Therefore, the search for safe and effective treatment strategies for RA, focusing on SFs as therapeutic targets to block synovial hyperplasia and bone erosion, has become an urgent problem to be solved. Therefore, research on safe and effective treatment strategies for RA has become an urgent problem to be solved in order to relieve the burden it brings to patients, families, and society.

MicroRNAs (miRNAs) are a class of endogenous evolutionarily conserved small molecule single-stranded non-coding RNAs [4]. Their main function is to negatively regulate the expression of target genes by inhibiting transcription or direct cleavage of mRNA. Abnormal expression of miRNA is closely related to the occurrence and development of diseases and plays an important regulatory role in various stages of immune cell maturation and immune homeostasis. Therefore, miRNA is becoming a new target for studying the mechanism of RA and its treatment. miRNAs are known to be involved in the regulation of almost all biological processes, including the inflammatory response of RA, the proliferation of SFs, and the production of cytokines. In addition to their regulatory function, miRNAs can be transmitted in the form of Exosoms (Exos) transport. Mesenchymal stem cell-derived Exos (MSC-Exos) are a form of extracellular vesicles produced by MSCs. MSC-Exos have a diameter of 40-100 nm and contain a rich array of biological information transfer media including proteins, mRNA, miRNA, and other biologically active substances. MSC-Exos retain the functions of MSCs and have advantages that MSCs lack, making them a potential strategy for stem cell treatment of diseases. MSC-Exos can transmit miRNA and "reprogram" target genes, thereby regulating behaviors such as proliferation, differentiation, and apoptosis of target cells [5,6]. This form of miRNA transport is a novel mechanism of cell communication. The discovery of the mechanism of directional transport of miRNA in organisms, combined with the efficient delivery mode of Exos and their structural characteristics of easy preservation and regulation, provides new possibilities for therapeutic and transformational applications [7]. Moreover, it offers new ideas for targeted therapy using miRNA. Therefore, the miRNA contained in MSC-Exos may be the key molecular mechanism underlying the various biological effects of MSC-Exos.

This study explores the therapeutic potential of exosomes derived from hUCMSCs with the aim of addressing RA both in vivo and in vitro. This research contributed to the growing body of evidence supporting the potential utility of hUCMSC-Exos in the treatment of RA and the promising prospects of miRNA-targeted therapy.

#### 2. Materials and methods

## 2.1. Ethics statement

Signed informed consent was obtained from all participants prior to enrolment in the study. The study followed the tenets of the Declaration of Helsinki and was approved by the Ethical Committee of the Shanxi Bethune Hospital (ethical approval code: 2018LL007).

## 2.2. Isolation, culture, and identification of hUCMSCs

The umbilical cord tissue of healthy full-term newborns was washed with PBS under sterile conditions. The umbilical vein and umbilical artery were then removed, followed by the removal of the Huatong gum

tissue. Subsequently, the tissue was cut into blocks of approximately 0.5 cm<sup>3</sup> in size. The culture method employed was tissue adherence, with the addition of serum-free medium. The cells were then incubated in a 37 °C and 5 % CO<sub>2</sub> incubator for a period of 20–25 days. Once the cells reached 80 % confluency, they were passaged at a 1:3 ratio. The P3 generation hUCMSCs with 80 % confluency were selected. These cells were digested with trypsin without EDTA, the digestion was terminated, and then centrifuged and resuspended. After counting, two tubes of single-cell suspensions with a concentration of 1  $\times$  10 $^{\circ}$ 6/mL were prepared. These were divided into a blank control group and a test sample group. After filtration and centrifugation, the supernatant was discarded, and the cells were gently resuspended by tapping the bottom of the tube. A 100  $\mu$ L single-cell suspension containing PE or FITC-labeled murine anti-human monoclonal antibodies CD105, CD73, CD90, CD45, CD34, HLA-DR (Abcam, USA) was added to the cell suspensions. The cells were incubated in the dark for 30 min. Subsequently, 3 mL of PBS was added for washing, followed by centrifugation at 1500 rpm for 5 min. The supernatant was discarded, and the cells were resuspended in 200 µL of PBS. The cells were then filtered through a mesh, gently tapped at the bottom of the tube to ensure uniformity, and both the blank control group and the test sample group were analyzed using the flow cytometry (ACEA, USA).

To assess the multipotent differentiation potential of hUCMSCs, the cells were were transferred into a 6-well plate and cultured separately in osteogenic induction medium (OriCell, China), adipogenic induction medium (Transgen, China), and chondrogenic induction medium (Transgen, China) for a period of 21 days. These distinct culture media were employed to facilitate differentiation towards osteogenic, adipogenic, and chondrogenic lineages, respectively. Alizarin Red staining was performed to assess the osteogenic potential of the cells. For the analysis of adipogenic potential, Oil Red O staining was conducted. To evaluate the chondrogenic potential, Methylaniline Blue staining was performed.

## 2.3. Preparation and characterization of hUCMSC-Exos

The hUCMSCs were cultured in FBS-free media for 72 h before collecting the medium. After culturing, the exosomes from the supernatant were separated through gradient ultra-high-speed centrifugation at 4  $^{\circ}$ C. The centrifugation process involved multiple steps, starting with a centrifugation rate of 300g and a duration of 10 min. This was followed by centrifugation at 2000g for 10 min, then at 10,000g for 30 min, and finally at 100,000g for 70 min. The separated Exos were suspended in PBS. To conduct TEM analysis, start by gently resuspending the microvesicle pellet in a suitable buffer or medium, ensuring proper dilution of the Exos. Apply a small drop of 10  $\mu$ L of the resuspended sample onto a carbon-coated TEM grid, specifically choosing a copper mesh for sample loading. Allow the sample to settle for 5 min, ensuring that any excess liquid is absorbed using filter paper. For negative staining, add 20 µL of 0.2 % aqueous phosphotungstic acid, allowing it to settle for 5 min before absorbing any excess stain with filter paper. Allow the grid to airdry under an incandescent lamp, or use a gentle stream of nitrogen to remove any remaining liquid. Once the grid is dry, ensure proper alignment and place it in the TEM sample holder. Then, insert the grid into the transmission electron microscopy (TEM) (JEOL, Japan) and adjust the imaging parameters for optimal visualization of the microvesicles. Finally, capture the electron micrographs by exposing the sample to a focused electron beam, completing the TEM analysis. Exos were diluted 1:20 with PBS and thoroughly mixed by pipetting, then analyzed using nanoparticle tracking analysis (NTA) (Particle Metrix, Germany). Ensure that the loaded cuvette or capillary is thoroughly mixed by pipetting and properly aligned with the laser beam. Once the instrument is ready, allow it to capture the data by analyzing the Brownian motion of particles. For nanoparticle size analysis, Exos were diluted 1:50 with PBS, mixed well by pipetting, and analyzed using the system from Malvern, UK. The protein concentration of the Exos was

determined using the BCA Protein Concentration Assay Kit (Solarbio, China). Finally, the antigen phenotypes of the Exos surface proteins, including CD9, CD63 and TSG101 (Abcam, USA) were detected using Western blot.

#### 2.4. Isolation, culture, and identification of RA SFs

Synovial tissue was collected from RA patients undergoing arthroscopy or arthroplasty under sterile conditions. The collected tissue was rinsed with PBS and then cut into approximately 1 mm<sup>3</sup> pieces. Subsequently, the synovial tissue was trypsinized with 0.25 % trypsin/EDTA (Solarbio, China) for 1 h. After trypsinization, the tissue was incubated in complete medium, which consisted of Dulbecco's Modified Eagle Medium (DMEM) (Gibco, USA) supplemented with 10 % fetal bovine serum (FBS) (Gibco, USA) and 1 % antibiotic-antimycotic solution (Solarbio, China), in a 5 % CO2 incubator at 37 °C for 21 days. Once the RA SFs reached 80 % confluency, they were trypsinized, centrifuged, and then passaged at a 1:2 ratio. To identify specific cell surface markers, a single cell suspension of RA SFs was prepared and labeled with PE or FITC-labeled murine anti-human monoclonal antibodies targeting cadherin 11 (CDH 11) (Abcam, USA), Podoplanin (PDPN) (Abcam, USA), and CD68 (Abcam, USA). Flow cytometry was used to detect these labeled antibodies in a 100  $\mu L$  cell suspension.

### 2.5. HUCMSC-Exos targets RA SFs

HUCMSC-Exos were labeled with RNA SelectTMGreen Fluorescent Cell Stain (Thermo Fisher Scientific Inc., USA) working solution and incubated at 37  $^{\circ}\text{C}$  for 20 min, protected from light. Then hUCMSC-Exos residual dye was removed using Exo Spin Columns. HUCMSC-Exos and RA SFs were incubated together for 24 h, also under protection from light. Afterward, Hoechst 33342 was added and incubated in the dark for 10 min. The film was then cleaned and sealed, and the fluorescence was observed.

#### 2.6. Effects of hUCMSC-Exos on the biological function of RA SFs

Real-time cell analysis (RTCA) (Agilent Technology, USA) was used to detect the effects of hUCMSC-Exos on the proliferation, migration, and invasion of RA SFs. For cell proliferation assays, the impedance change caused by proliferating cells was measured in real-time by microelectronic biosensors. RA SF suspension (3  $\times$  10<sup>3</sup> cells/well) was seeded into E-Plate 16 (Roche, Switzerland), and hUCMSC-Exos (0 µg/ mL, 30 μg/mL, 90 μg/mL, 150 μg/mL) was added 6 h later. To observe the cell migration and invasion experiments were conducted using the C-Plate 16 (Roche, Switzerland). In the migration experiments, the lower chamber of C-Plate 16 was filled with medium containing 15 % FBS, while the upper chamber was filled with a suspension of RA SFs prepared with different concentrations of hUCMSC-Exos serum-free medium  $(2.5 \times 10^3 \text{ cells/well})$ . The movement of RA SFs through a microporous membrane was monitored by a biosensor at the bottom of the lower chamber containing 15 % FBS in the medium for 48 h. As for invasion experiments, the C-Plate 16 was pre-coated with a 1:40 dilution of matrigel and monitored for 72 h. The electrode impedance was displayed as a proliferation, migration, or invasion index.

## 2.7. Effects of miRNAs in hUCMSC-Exos on the biological function of RA SFs

## 2.7.1. Preparation of $hUCMSC^{KD-AGO2}$

The experiment started with seeding a 100  $\mu$ L hUCMSCs cell suspension (5  $\times$  10<sup>4</sup> cells/mL) in 96-well plates, resulting in approximately 20 % cell confluency after 24 hoursours. The experiment was then divided into four groups: Group A as the blank control group, Group B as the negative control with the addition of complete medium, Group C with the addition of infection enhancement fluid HitransG A

(Genechem, China) to complete medium, and Group D with the addition of infection enhancement fluid HitransG P (Genechem, China) to complete medium. To determine the optimal infection conditions for transfection, the viral infection plural number was calculated using the equation  $MOI = (viral\ titer \times virus\ volume) / number of\ cells.$  Lentivirus (LV) was added to the complete medium, creating four different gradients of MOI (1, 10, 50, 100) in the infection group. After incubating for 16 h at 37 °C and 5 % CO<sub>2</sub>, the medium was changed and infected for 72 h. The fluorescence expression was observed to determine the effectiveness of the infection conditions for transfection. The construction of  $\ensuremath{\text{hUCMSC}^{\text{KD-AGO2}}}\xspace$  consisted of four groups: KD1 group infected hUCMSCs with LV-AGO2-RNAi (85384-1): gcACAGCCAGTAATCGAGTTT, KD2 group infected hUCMSCs with LV-AGO2-RNAi (85385-11): cgGCAA-GAAGAGATTAGCAAAA, KD3 group infected hUCMSCs with LV-AGO2-RNAi (85386-11): caATCAAATTACAGGCCAATT, and the negative control (NC) group infected hUCMSCs with the negative control viral vector (RNAi-NC-LV) (TTCTCCGAACGTGTCACGT). The cell status of each group was ensured to be good during the transfection process. After 16 h of infection, the cells from each well were collected and transferred to T25 flasks, with the addition of an appropriate amount of complete medium. The fluorescence rate was observed 72 h after infection to determine the positive infection rate.

## 2.7.2. AGO2 gene and protein expression in $hUCMSC^{KD-AGO2}$

The total RNA and isopropanol precipitated RNA in hUCMSC KD-AGO2 and hUCMSC<sup>NC</sup> were extracted using TRIzol reagent (Thermo Fisher Scientific Inc., USA). The expression of AGO2 was analyzed by RT-PCR. The concentration and quality of the extracted RNA were determined by Nanodrop2000/2000C spectrophotometer analysis ((Thermo Fisher Scientific Inc., USA)) after adding RNase-free water (TAKARA, Japan) to the precipitation until completely dissolved. To analyze mRNA expression levels and DNA synthesis, the phosphoglyceraldehyde dehydrogenase gene (GAPDH) was used as an internal control for each sample experiment. The primer sequences for GAPDH and AGO2 were used for F5'-TGACTTCAACAGGACACCCA-3', RT-PCR: GAPDH: CACCCTGTTGCTGTAGCCAAA-3': F5'-TCCACCTA-AGO2: GACCCGACTTT-3', R5'-GTTCCACGATTTCCCTGTT-3'. For Western blotting analysis of AGO2 in hUCMSCsKD-AGO2, the proteins were separated on a 10 % sodium dodecyl sulfate-polyacrylamide gel electrophoresis gel and transferred to a polyvinylidene fluoride membrane (Millipore, USA). The membrane was blocked in 5 % fat-free dry milk for 2 h and then incubated overnight with antibodies to Anti-AGO2 (SantaCruz, USA) diluted at 1:1000. After that, the membrane was incubated with goat anti-rabbit IgG-HRP (SantaCruz, USA) (1:2000) for 2 h.

## 2.7.3. Preparation and characterization of $hUCMSC^{KD-AGO2}$ -Exos

Exos were separated by gradient ultracentrifugation, followed by visualization through TEM. The size of Exos particles was detected using NTA and nanoparticle size analysis. The protein concentration of Exos was determined using the BCA Protein Concentration Assay Kit (Solarbio, China). The antigen phenotypes of Exos surface, including CD9, CD63, and TSG101(Abcam, USA), were detected using the Western blot method.

2.7.4. Effects of hUCMSC<sup>KD-AGO2</sup>-Exos on the biological function of RA SFs RA SFs were respectively co-cultured with 150  $\mu$ g/mL hUCMSC<sup>KD-AGO2</sup>-Exos and 150  $\mu$ g/mL hUCMSC<sup>NC</sup>-Exos. RASFs proliferation and migration experiments were detected using RTCA, and invasive ability was assessed using transwell.

## 2.7.5. Differences in miRNAs before and after the intervention of hUCMSC-Exos in RA SFs

The P3 generation RA SFs in 6 patients were used to screen for differential miRNAs before and after hUCMSC-Exos intervention. The RASF after the hUCMSC-Exos intervention was labeled RA SF $^{\rm Exo}$ . The RASF before the hUCMSC-Exos intervention was labeled RA SF $^{\rm Ctrl}$ . Total RNA

was extracted using the mirVana miRNA Isolation Kit (Ambion) following the manufacturer's protocol. The Nanodrop 2000 (Thermo Fisher Scientific Inc., USA) was used to quantify the total RNA, while the RNA integrity was assessed using the Agilent 2100 Bioanalyzer (Agilent Technology, USA). For small RNA library construction, 1 ug of total RNA from each sample was utilized with the TruSeg Small RNA Sample Prep Kits (Illumina, USA). The manufacturer's recommendations were followed, involving ligation of adapters to the total RNA, reverse transcription of the adapter-ligated RNA to cDNA, and PCR amplification. The small RNA library was isolated and purified, and library quality was assessed on the Agilent Bioanalyzer 2100 system with DNA High Sensitivity Chips. Subsequently, the libraries underwent sequencing with the Illumina HiSeq X Ten platform, generating 150 bp paired-end reads. We conducted the small RNA sequencing and analysis. The base calling process converted the basic reads into sequence data, and lowquality reads were filtered out. Reads with 5' primer contaminants and poly(A) were removed as well. Additionally, reads without 'adapter and insert tag, those shorter than 15 nt or longer than 41 nt, were discarded to obtain clean reads. Primary analysis involved determining the length distribution of the clean sequences in the reference genome. The noncoding RNAs were annotated as rRNAs, tRNAs, and small nuclear RNAs (snRNAs), among others. The annotation process involved aligning the RNAs with fam v.10.1 (https://www.sanger.ac.uk/softw are/Rfam). Known miRNAs were identified by aligning against the miRBase v22 database (https://www.mirbase.org/) for subsequent analysis of their expression patterns. Additionally, unannotated reads were analyzed using mirdeep2 to predict novel miRNAs. The corresponding miRNA star sequence and miRNA mature sequence were also identified based on the hairpin structure of a pre-miRNA and the miR-Base database. Differentially expressed miRNAs were calculated and filtered using a threshold of P value < 0.05, along with the p value calculated using the DEG algorithm for experiments with biological replicates and the Audic Claverie statistic for experiments without biological replicates. The software miRBase, TargetScan, miRTarBase were used to predict the targets of differentially expressed miRNAs. Finally, GO enrichment and KEGG pathway enrichment analyses of differentially expressed miRNA-target-Gene were performed using R based on the hypergeometric distribution.

## 2.7.6. hUCMSC-Exos regulated the transmission of miRNAs between hUCMSCs and RASFs

Chemically defined media (CdM) with or without GW4869 (Med-ChemExpress, USA) (CdM<sup>GW4869</sup> or CdM<sup>MSC</sup>) was collected after incubating hUCMSC for 24 h. The miRNAs of RA SF were extracted following the intervention of CdM<sup>GW4869</sup>, CdM<sup>MSC</sup> and 150ug/mL hUCMSC-Exos in RA SF for 48 h. The concentration and purity of miRNA were detected. cDNA was synthesized using a reverse transcriptase kit (Thermo Fisher Scientific Inc., USA). We designed miRNA primers using the

**Table 1** Sequence of U6 and miRNAs.

Primers	Accession	Sequence ( 5'-3' )
U6		F:5'-GCTCGCTTCGGCAGCACATATAC-3'
U6		R:5'-CGAATTTGCGTGTCATCCTTGCG-3'
hsa-miR-7-5p	MIMAT0000252	F:5'-AAGAGCGTTGGAAGACTAGTGATT-3'
hsa-miR-181b-5p	MIMAT0000257	F:5'-ACACTACGAACATTCATTGCTGTC-3'
hsa-miR-186-5p	MIMAT0000456	F:5'-AAGCGACCCAAAGAATTCTCCTT-3'
hsa-miR-146a-5p	MIMAT0000449	F:5'-AGCTGGACTGAGAACTGAATTCC-3'
hsa-miR-155-5p	MIMAT0000646	F:5'-AAGCGCCTTTAATGCTAATCGTG-3'
hsa-miR-222-3p	MIMAT0000279	F:5'-ACACTACGAGCTACATCTGGCT-3'
hsa-miR-320-3p		F:5'-AACACGCAAAAGCTGGGTTGA-3'
hsa-miR-1193	MIMAT0015049	F:5'-ACGAGAACGGGATGGTAGACC-3'
hsa-miR-1307-3p	MIMAT0005951	F:5'-TATAGACTCGGCGTGGCGTC-3'
hsa-miR-3529-3p	MIMAT0022741	F:5'-AGCGCCTAACAACAAAATCACTAG-3'
hsa-miR-451a	MIMAT0001631	F:5'-AGGCGCATAAACCGTTACCATT-3'
hsa-miR-382-5p	MIMAT0000737	F:5'-AACAAGGAAGTTGTTCGTGG-3'
hsa-miR-27a-5p	MIMAT0004501	F:5'-AAGCACAGGTAGCTGCT-3'

tailing method, with only forward sequences (Table 1). RT-qPCR amplification was performed using the SYBR Green Master Mix kit (MedChemExpress, USA) with cDNA as a template. Each sample was set up with 3 complex wells with 20  $\mu$ L of reaction system. U6 was used as an internal reference. The relative expression level of target miRNA in RA SF was calculated and analyzed by the relative quantitative  $2-\Delta\Delta$ Ct method, in comparison with the control group.

### 2.7.7. Effect of miR-451a on RA SFs

The miR-451a mimics plasmid and NC mimics plasmid were used to construct RA SF  $^{\rm miR-451a}$  and RA SF  $^{\rm NC}$ , respectively. (miR-451a mimics:F 5′-AAACCGTTACCATTACTGAGTT-3′. NC mimics:F 5′-TTCTCCGAACG TGTCACGT-3′). GP-transfectect-Mate transfection reagent was used for initial transfection, and after 4–6 h, we replaced the transfection reagent with a complete medium. mRNA expression was detected after 24–72 h. The target gene for miR-451a, ATF2, was identified through miRBase, TargetScan, and miRTarBase.

To determine the interaction between luciferase reporter genes, we first synthesized a luciferase reporter plasmid (Promega, USA) by inserting the *ATF2* fragment carrying the miR451a binding site. This plasmid was labeled as *ATF2* wild-type (wt). Additionally, we synthesized another luciferase reporter plasmid, labeled as *ATF2* mut, which contained a mutated miR-451a binding site. We then used Lipofectamine 2000 reagent (Invitrogen, USA) to transfect the cells. After 48 h, we evaluated luciferase activity using the dual luciferase reporter assay system (Promega, USA).

The expression levels of miR-451a and target gene ATF2 in RA SF<sup>miR-451a</sup> were measured using the RT-qPCR method (ATF2: F5′-GGTCATGGTAGCGGATTGGTTAGG-3′, R5′-GTAGTGGATGTGGCTGGCTGTTG-3′, GAPDH: F5′-CTTTGGTATCGTGGAAGGACTC-3′, R5′-GTAGAGGCAGGATGATGTTCT-3′). Western blot analyzed the ATF2 protein in RA SF<sup>miR-451a</sup>. We assessed the proliferation of RA SF<sup>miR-451a</sup> using the CCK8 method and the migration ability using the cell scratch experiment. The invasion of RA SF<sup>miR-451</sup> a was evaluated through the Transwell experiments.

## 2.8. Preparation of hUCMSC-Exos<sup>miR-451a</sup>

As described in the exosomal RNA loading kit (Echo biotech, China), we loaded miR-451a into hUCMSCs. Firstly, 1 mL ETP solution was added to the dry powder of the Exo transporter (ETP). Sequentially, miR-451a, hUCMSCs-Exo, and ETP were added, and the final reaction solution was adjusted to a volume of 600  $\mu L$ . The reaction solution was then incubated at 37  $^{\circ} C$  in the dark for 2 h, with continuous shaking at 150 rpm. Next, the incubated sample was transferred to an ultrafiltration tube to remove free oligonucleic acids. It was then washed twice with Washing Buffer, resulting in the obtainment of miR-451a loaded Exos from hUCMSCs (hUCMSC-Exos^miR-451a).

## 2.9. Effect of hUCMSC-Exos<sup>miR-451a</sup> on RA SFs

 $150~\mu g/mL~hUCMSC\textsc{-}Exos$  were incubated with RA SF for 48 h, and labeled as Exos group.  $150~\mu g/mL~hUCMSC\textsc{-}Exos^{miR\textsc{-}451a}$  were incubated with RA SF for 48 h, and labeled as Exos^{miR\textsc{-}451a} group. RT-qPCR detected miR-451a and ATF2 expression levels in RA SFs.Western blot analyzed the ATF2 protein in RA SFs. The proliferation ability of RA SFs was detected by CCK8 method. The migration of RA SFs was detected by cell scratch experiment, and the invasion of RA SF was detected by Transwell experiment.

## 2.10. Effect of hUCMSC-Exos<sup>miR-451a</sup> on CIA rats

The female Wistar rats, aged 6-8 weeks and weighing 180-200 g, were obtained from the experimental animal center of Shanxi Provincial People's Hospital. The rats were subsequently housed in the Shanxi Bethune Animal Center in conditions that were maintained at a

controlled temperature of 20 degrees Celsius, a relative humidity of 50 %, and a photoperiod of 8 h.All experiments were conducted in accordance with the guidelines of the animal protection and use committee of Shanxi Medical University.

The rats were segregated into the normal group (n = 6) and the CIA model group (n = 18). Rat models of CIA were generated through immunization with type II collagen. Briefly, upon anesthesia with isoflurane, the rats were injected with mixed emulsions containing 0.1 mL of complete Fresno adjuvant and 400 µg of bovine type II collagen (SigmaAldrich, USA) on the dorsa, the root of the tail. The rats in the blank group were similarly administered physiological saline. After 2 weeks, CIA model rats were intraperitoneally administered a 0.2 mL emulsion containing 1 mg/mL bovine type II collagen for booster immunization. The blank group was administered the same amount of physiological saline. The thirty-two CIA rats were randomly assigned to four groups: CIA control group (CIA group, n = 6), hUCMSCs-Exos intervention group (hUCMSCs-Exos group, n = 6) and hUCMSCs-Exos- $^{
m miR-451a}$  intervention group (BMSC group, n=6). In the hUCMSCs-Exos intervention group,hUCMSCs-Exos were transplanted into the ankle joint cavities of each rat once after booster immunization. In the hUCMSCs-Exos<sup>miR-451a</sup> intervention group, hUCMSCs-Exos<sup>miR-451a</sup> were transplanted into the ankle joint cavities of each rat once after booster immunization. The normal group and CIA model group, as the control groups, were similarly administered an equal volume of normal saline at the same time point. Each group was housed separately throughout the

To evaluate joint inflammation and joint destruction in CIA model rats in the CIA group, hUCMSCs-Exos group and hUCMSCs-Exos<sup>miR-451a</sup> group, assessment of arthritis index (AI), imaging, and pathological analysis were performed. Joint inflammation was assessed via AI weekly from primary immunization to 5 weeks after intervention at eight time points. AI was graded on a scale of 0-4: 0 = no evidence of hyperemia and/or inflammation; 1 = hyperemia with minor or no paw swelling; 2 = swelling confined predominantly to the ankle region, with modest hyperemia; 3 = increased paw swelling and hyperemia of the ankle and metatarsal regions; and 4 = maximal paw swelling and hyperemia involving the ankle, metatarsal, and tarsal regions. The scores of four hind paws were combined to obtain the AI for each rat, with a maximum possible score of 16. Micro-computed tomographic (micro-CT) assessment (SCANCO Medical AG, Switzerland) of joint destruction were conducted on 1 month after intervention independently by two experienced physicians in a blinded manner. For histological analysis, rats were euthanized via cervical dislocation. Organ tissues include synovial tissue, heart tissue, liver tissue, spleen tissue, lung tissue, kidney tissue were randomly harvested, embedded in paraffin, sectioned, and stained with hematoxylin and eosin. The expression of miR-451a and ATF2 in synovial tissue was detected by RT-PCR. Western blot analyzed the expression of ATF2 protein in synovial tissue. We used a fully automated biochemical analyzer (Thermo Fisher Scientific, USA) and biochemistry detection kit (ZECEN Biotech, China) to measure the levels of alanine transferase (ALT), aspartate transferase (AST), alkaline phosphatase (ALP), total protein (TP), albumin (ALB), urea nitrogen (BUN), uric acid (UA), and creatine kinase (CK) in rat blood.

### 2.11. Statistical analysis

GraphPad Prism 8.0 was used to perform statistical analysis. All data are expressed as the mean standard deviation and were evaluated by analysis of variance (ANOVA). Non-normally distributed data are expressed as the median(quartile spacing). Kruskal-Wallis and Wilcoxon rank sum tests were used to evaluate data from intergroup overall comparisons and sample pairs, respectively. P values 0.05 were considered statistically significant.

#### 3. Results

## 3.1. Characterization of hUCMSCs, hUCMSC-Exos and RA SFs, and the effect of hUCMSC-Exos on RA SFs

HUCMSCs cultured by substrate adhesion displayed a long spindle-like morphology (Fig. 1a). Flow cytometry analyses of the surface antigen phenotype of hUCMSCs revealed the expression of CD105, CD73, CD90, but not CD45, CD34, CD31 (Fig. 1b). Moreover, upon culturing in an induction medium, hUCMSCs possessed osteogenic (Fig. 1c), adipogenic (Fig. 1d) and chondrogenic differentiation (Fig. 1e) potentials in vitro.

TEM revealed that hUCMSC-Exos were oval phospholipid bilayer-bound structures with diameters in the range of 30–150 nm (Fig. 1f). NTA showed that the diameter distribution of hUCMSC-Exos was a single peak, the median particle diameter was 122 nm, and the concentration was  $9.2\times10^6$  particles/mL (Fig. 1g). Highly sensitive nanoparticle size analyses indicated the particle size distributions of hUCMSC-Exos as single peaks, with peak value 122 nm (Fig. 1h). The protein concentrations of hUCMSC-Exos were 1.384 µg/µL. Western blot confirmed the expression of CD9, CD63 and TSG101 in hUCMSC-Exos. (Fig. 1i). RA SFs cultured by substrate adhesion displayed a fibroblast-like morphology (Fig. 1j). Flow cytometry analyses of the surface antigen phenotype of RA SFs revealed the expression of PDPN and CDH-11, but not CD68 (Fig. 1k).

The hUCMSC-Exos delivered RNA to RA SFs. Subsequent to mixing and 24 h incubation of green fluorescent-labeled RNA-containing hUCMSC-Exos and RA SFs, it was observed that the blue-stained nuclei of RA SFs had accumulated green fluorescence. This indicates that RA SFs can uptake the RNA of hUCMSC-Exos (Fig. 11). hUCMSC-Exos inhibits the RA SFs phenotype. After 6 h of inoculation, all RA SFs adhered to the substrate. The cell index proliferation curve flattened after 25 h. hUCMSC-Exos inhibited the proliferation of RA SFs at different times, with 150 mg/mL being the most effective (Fig. 1m). The cell migration curve shows hUCMSC-Exos inhibited the migration of RA SFs at different times, with 150 mg/mL being the most effective (Fig. 1n). hUCMSC-Exos inhibited the invasion of RA SFs, with 150 mg/mL being the most effective (Fig. 1o).

## 3.2. Effects of miRNAs in hUCMSC-Exos on RA SFs

## 3.2.1. Preparation of $hUCMSC^{KD-AGO2}$

hUCMSCs were infected with LV-AGO2-RNAi (85384-1), LV-AGO2-RNAi (85385-11), LV-AGO2-RNAi (85386-11), RNAi-NC-LV, respectively (Fig. 2a).

The expression abundance of AGO2 in hUCMSCs was high, and the average value of  $\triangle$ Ct was 9.73. RT-PCR determined the highest knockdown efficiency of the AGO2 in hUCMSCs<sup>KD3-AGO2</sup> (P < 0.0001) (Fig. 2b). Western blot analysis determined the lowest level of AGO2 expression in hUCMSCs<sup>KD3-AGO2</sup>(Fig. 2c).We prepared hUCMSCs<sup>KD3-AGO2</sup> from LV-AGO2-RNAi (85386-11) infected with hUCMSCs. The expression abundance of mature miRNAs is regulated by the transcribed AGO2 protein, and a decrease in AGO2 results in diminished expression and activity of mature miRNAs [8].

## 3.2.2. Characterization of hUCMSC KD-AGO2-Exos and hUCMSC NC-Exos

TEM showed hUCMSC<sup>NC</sup>-Exos and hUCMSC<sup>KD-AGO2</sup>-Exos are membranous vesicles with a diameter of 30–150 nm, with complete morphology and typical cup-tray morphology (Fig. 2d). NTA showed that the diameter distribution of hUCMSC<sup>NC</sup>-Exos was a single peak, the median particle diameter was 119 nm, and the concentration was  $9.9 \times 10^6$  particles/mL. The diameter distribution of hUCMSC<sup>KD-AGO2</sup>-Exos was a single peak, the median particle diameter was 111 nm, and the concentration was  $9.3 \times 10^6$  particles/mL (Fig. 2e). Highly sensitive nanoparticle size analyses determined the particle size distributions of hUCMSC<sup>NC</sup>-Exos and hUCMSC<sup>KD-AGO2</sup>-Exos as single peaks.The peak

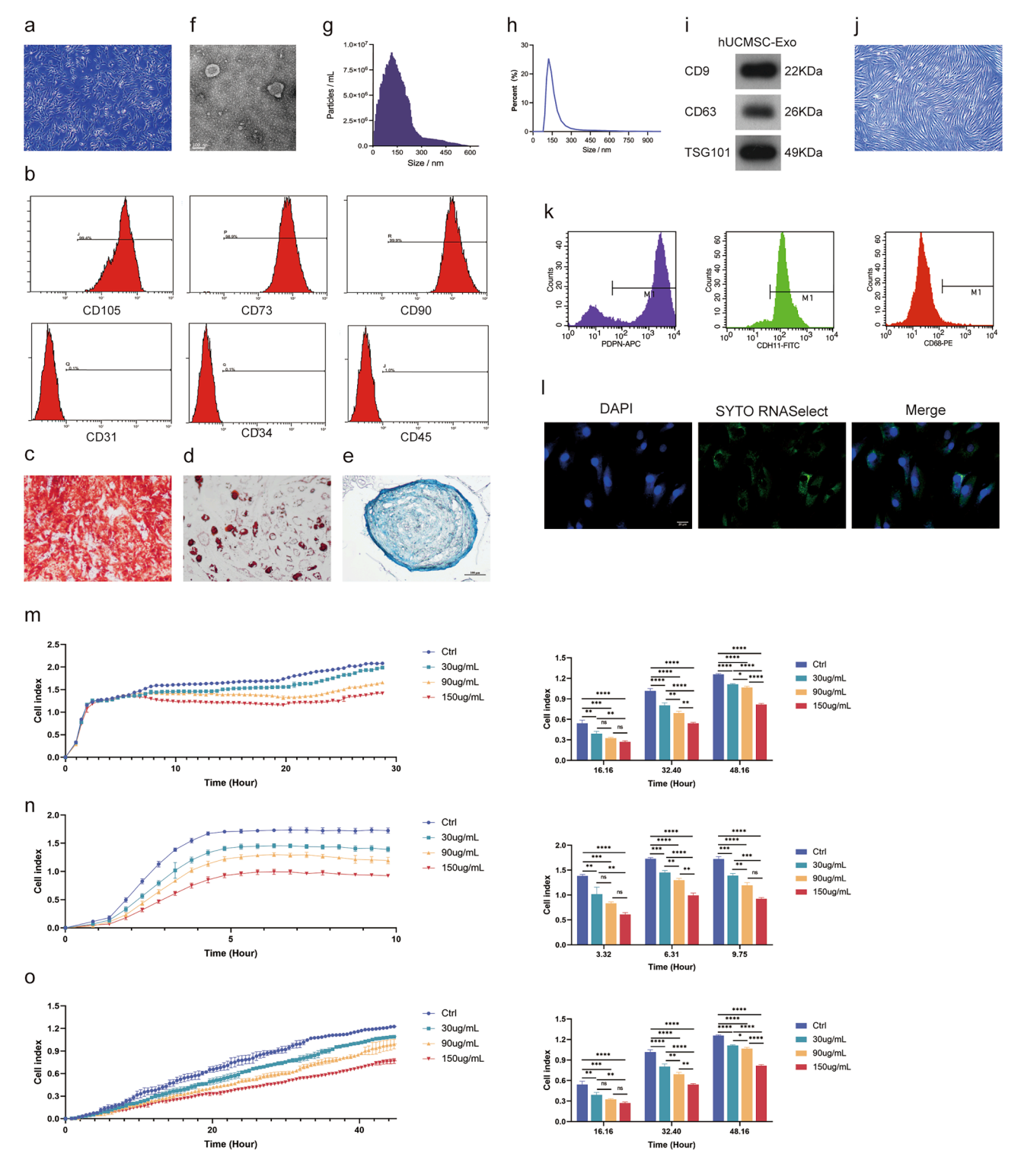


Fig. 1. Characterization of hUCMSCs, hUCMSC-Exos and RA SFs, and the effect of hUCMSC-Exos on RA-SFs. (a) hUCMSCs exhibited a long spindle-like morphology  $(40\times)$ . (b) Flow cytometry results showed that hUCMSCs were positive for CD105, CD73, CD90, while negative for CD45, CD34, CD31. (c) Osteogenic differentiation of hUCMSCs indicated by Alizarin Red staining  $(40\times)$ . (d) Oil red O staining of hUCMSCs after induction of adipogenic differentiation  $(40\times)$ . (e) Chondrogenic differentiation of hUCMSCs indicated by toluidine blue staining  $(100\times)$ . (f) Transmission electron microscopy of isolated hUCMSC-Exos  $(20,000\times)$ . (g) NTA determined the size distribution of hUCMSC-Exos. the median diameter of the particles (115 nm) and their concentration  $(9.2\times10^6 \text{ particles/mL})$ . (h)Highly sensitive nanoparticle size analyses determined the particle size distributions of hUCMSC-Exos. (i) Western blot analysis showed that hUCMSC-Exos express CD9, CD63 and TSG101. (j) RA SFs exhibited a fibroblast-like morphology  $(40\times)$ . (k) Flow cytometry results showed that RA SFs were positive for PDPN and CDH-11, while negative for CD68. (l) RA SFs took up the RNA of hUCMSC-Exos. (m) hUCMSC-Exos inhibited the proliferation of RA SFs, with 150 mg/mL being the most effective. (o) hUCMSC-Exos inhibited the invasion of RA SFs, with 150 mg/mL being the most effective. (o) hUCMSC-Exos inhibited the invasion of RA SFs, with 150 mg/mL being the most effective. (o) hUCMSC-Exos inhibited the invasion of RA SFs, with 150 mg/mL being the most effective. (e) hUCMSC-Exos inhibited the invasion of RA SFs, with 150 mg/mL being the most effective. (e) hUCMSC-Exos inhibited the invasion of RA SFs, with 150 mg/mL being the most effective.

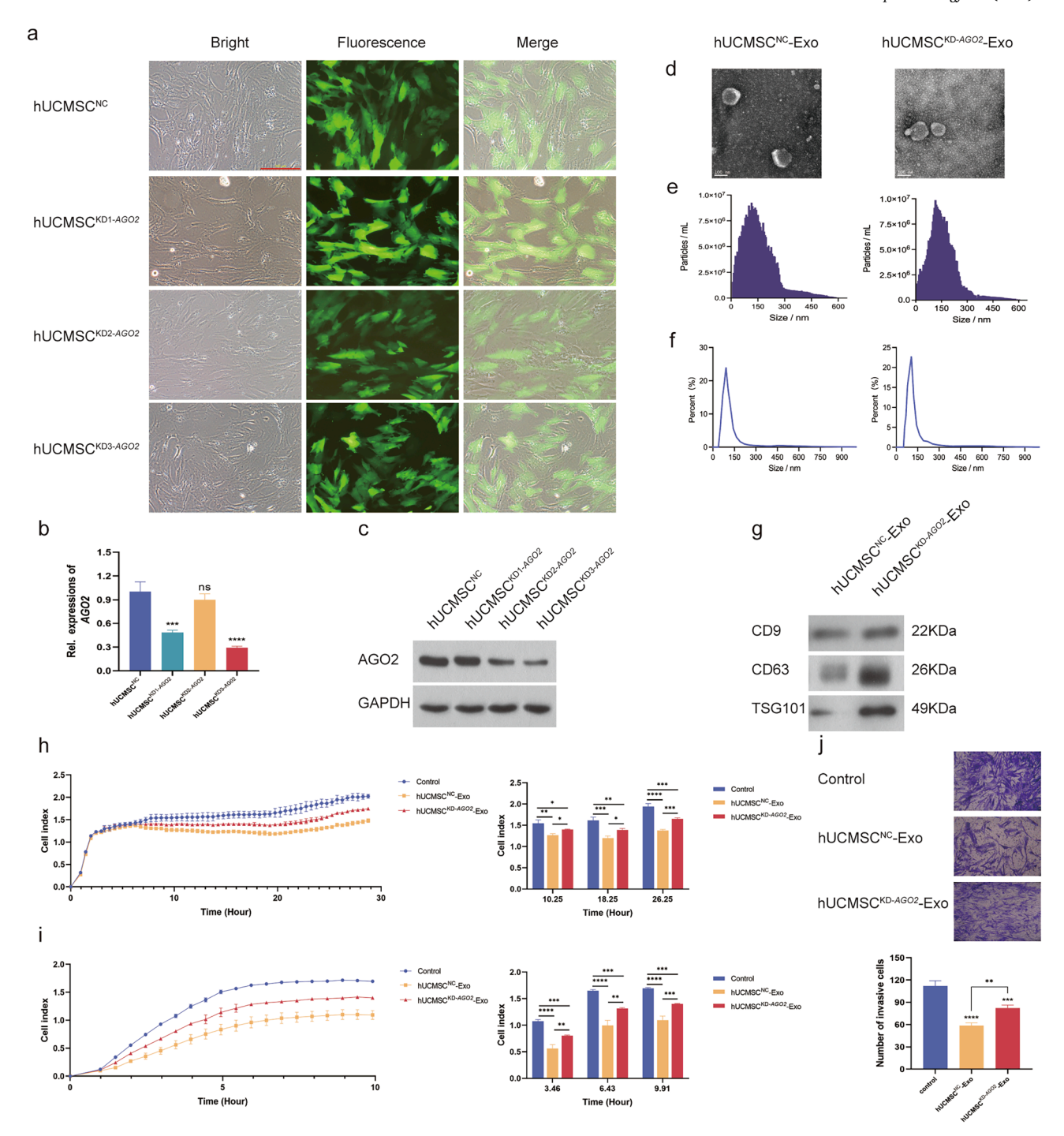


Fig. 2. Effects of miRNAs in hUCMSC-Exos on RA SFs. (a) hUCMSCs were infected with LV-AGO2-RNAi (85384-1), LV-AGO2-RNAi (85385-11), LV-AGO2-RNAi (85386-11), RNAi-NC-LV, respectively ( $100 \times$ ). (b) RT-PCR determined the highest knockdown efficiency of the AGO2 in hUCMSCs<sup>KD3-AGO2</sup>. (c) Western blot analysis determined the lowest level of AGO2 expression in hUCMSCs<sup>KD3-AGO2</sup>. (d) TEM of isolated hUCMSC<sup>NC</sup>-Exos and hUCMSC<sup>KD-AGO2</sup>-Exos. (20,000 $\times$ ). (e) NTA determined the size distribution of hUCMSC<sup>NC</sup>-Exos and hUCMSC<sup>NC</sup>-Exos express CD9, CD63 and TSG101. (h) At the same time, hUCMSC<sup>NC</sup>-Exos has a weaker inhibitory effect on the migration of RASFs at the same time. (j) At 48 h, hUCMSC<sup>NC</sup>-Exos had a weaker inhibitory effect on RASFs invasion than hUCMSC<sup>NC</sup>-Exos. \* P < 0.05, \*\* P < 0.01, \*\*\*\* P < 0.001, \*\*\*\* P < 0.0001.

value of hUCMSC  $^{NC}$ -Exos is 91.3 nm. The peak value of hUCMSC  $^{KD\text{-}AGO2}$ -Exos is 104 nm (Fig. 2f). Western blot analysis showed that hUCMSC  $^{NC}$ -Exos and hUCMSC  $^{KD\text{-}AGO2}$ -Exos express CD9, CD63 and TSG101 (Fig. 2g). The protein concentrations of hUCMSC  $^{NC}$ -Exos and hUCMSC  $^{KD\text{-}AGO2}$ -Exos were 1.133 µg/µL and 1.038 µg/µL, respectively.

3.2.3. Effects of miRNAs in hUCMSC-Exos on the biological function of RA SFs

The inhibitory effect of hUCMSC  $^{\text{KD-AGO2}}$ -Exos on the proliferation (P < 0.001) and migration (P < 0.001) of RA SFs was found to be weaker compared to hUCMSC  $^{\text{NC}}$ -Exos. Moreover, both hUCMSC  $^{\text{KD-AGO2}}$ -Exos and hUCMSC  $^{\text{NC}}$ -Exos demonstrated the ability to suppress the

proliferation (P < 0.001, P < 0.0001) and migration (P < 0.001, P < 0.0001) of RA SFs (Fig. 2h, Fig. 2i). After 48 h of intervention, it was observed that the hUCMSC<sup>NC</sup>-Exos group and the hUCMSC<sup>KD-AGO2</sup>-Exos group exhibited fewer RASF cells passing through the Transwell chamber in comparison to the hUCMSC-Exos group (P < 0.0001, P < 0.001).

Additionally, the hUCMSC AGO2-Exos group displayed a lesser number of RASF cells passing through the Transwell chamber compared to the hUCMSC CRC-Exos group (P < 0.01) (Fig. 2j). These findings suggest that the inhibitory effect of hUCMSC CRO-AGO2-Exos on the proliferation, migration, and invasion of RASFs is lower than that of hUCMSC CRC-Exos.

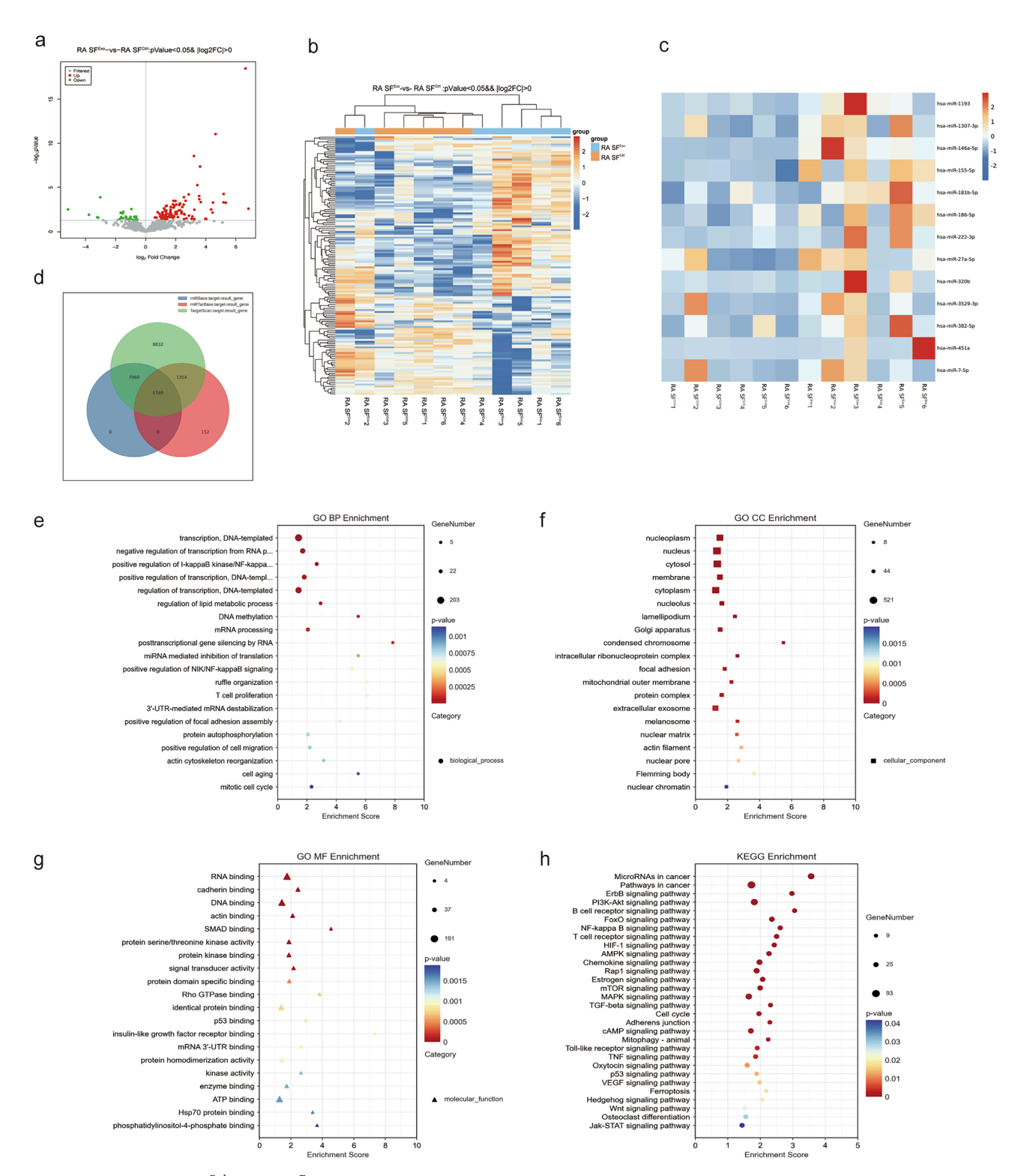


**Fig. 3.** Small RNA-seq for RA SF<sup>Exo</sup> and RA SF<sup>Exo</sup>, target genes for differential miRNAs and GO/KEGG analysis of target genes (a) The differential miRNAs were selected in RA SF<sup>Exo</sup> and RA SF<sup>Exo</sup> and RA SF<sup>Exo</sup>. (b) The clustering heatmap of differentially expressed miRNAs displayed significant differences in miRNAs between RA SF<sup>Exo</sup> and RA SF<sup>Ctrl</sup>. (c) There are 13 significantly different miRNAs by intersecting the upregulated miRNAs in RA SF<sup>Exo</sup> with all the miRNAs detected in hUCMSC-Exos. (d) 1749 intersecting target genes of 13 significantly different miRNAs were predicted. (e) (f) (g) GO analysis of target genes. BP: biological process, CC: cellular component, MF: molecular function. (h) KEGG analysis of target genes.

It can be inferred that miRNAs present in hUCMSC-Exos may have an impact on the proliferation, migration, and invasion of RA SFs.

## 3.2.4. Differences in miRNAs before and after the intervention of hUCMSC-Exos in RA SFs

The expression of miRNAs in RA  $SF^{Exo}$  and RA  $SF^{Ctrl}$  was quantified. Then, 139 differential miRNAs were selected based on  $|\log 2FC| > 0$  and P < 0.05 (Fig. 3a). The clustering heatmap of differentially expressed miRNAs displayed significant differences in miRNAs between RA  $SF^{Exo}$  and RA  $SF^{Ctrl}$ , demonstrating good reproducibility in the intra-group samples, except for RA  $SF^{Exo}$ 2 and RA  $SF^{Ctrl}$ 2 (Fig. 3b). We identified 13 significantly different miRNAs by intersecting the upregulated miRNAs in RA  $SF^{Exo}$  with all the miRNAs detected in hUCMSC-Exos (Fig. 3c). These miRNAs can be effectively transmitted to RA  $SF^{Exo}$  through hUCMSC-Exos. To predict their target genes, we utilized miRBase, TargetScan, and miRTarBase, resulting in 1749 intersecting genes (Fig. 3d).

Furthermore, the Gene Ontology (GO) and Kyoto Encyclopedia of Genes and Genomes (KEGG) pathway enrichment analyses were used to evaluate the intersecting genes. The top 20 participants in the Biological Process (BP) category were identified, which included posttranscriptional gene silencing by RNA miRNA (Fig. 3e). Additionally, the top 20 participants in the Cellular Component (CC) category were determined to include extracellular Exos (Fig. 3f). Finally, the top 20 participants in the Molecular Function (MF) category were found to have protein serine/threonine kinase activity (Fig. 3g). KEGG pathway enrichment analyses showed that pathways for signaling these target genes include:ErbB signaling pathway PI3K-Akt signaling pathway, B cell receptor signaling pathway, FoxO signaling pathway, NF-kappa B signaling pathway, T cell receptor signaling pathway, HIF-1 signaling pathway, AMPK signaling pathway [9], Chemokine signaling pathway, Rap1 signaling pathway, Estrogen signaling pathway mTOR signaling pathway, MAPK signaling pathway, TGF-beta signaling pathway, Adherens junction, cAMP signaling pathway, Toll-like receptor signaling pathway, TNF signaling pathway, p53 signaling pathway, VEGF signaling pathway, Ferroptosis, Hedgehog signaling pathway, Wnt signaling pathway, Osteoclast differentiation and Jak-STAT signaling pathway et al. (Fig. 3h). Most of these have been reported to be associated with RA, suggesting that these miRNAs may improve RA through these pathways.

## 3.2.5. UCMSC-Exos regulated the transmission of miRNAs between hUCMSCs and RASFs

After hUCMSC-Exos treatment, CdM  $^{GW4869}$  intervention, and CdM  $^{MSC}$  intervention in RA SF for 48 h, RT-qPCR detected that the 13 miRNAs screened by sequencing were significantly upregulated in RA SF in the hUCMSC-Exos group (P < 0.0001) and CdM  $^{GW4869}$  group (Fig. 4a). Among these miRNAs, miR-146a exhibited the largest variation, followed by miR-451a.

#### 3.2.6. Effect of miR-451a on RA SFs

Through TargetScan, the potential binding site of ATF2 was identified (Fig. 4b). The luciferase assay was conducted to directly assess the binding between miR-451a and ATF2. It was found that the pMiR reporter vector, which contained the miR-451a binding site of firefly luciferase and the 3'-UTR sequence corresponding to ATF2, caused a decrease in luciferase activity in cells transduced by miR-451a (P < 0.0001) (Fig. 4c). These findings indicate a direct binding between these two target genes. Furthermore, the targeted mutation at the binding site effectively eliminated the impact of miR-451a on luciferase activity. This suggests that miR-451a directly binds to the 3'-UTR of ATF2.

The transfection efficiency of miR-451a mimics and NC mimics in RA SF was assessed using RT-PCR after 24 h. The results showed a significant upregulation of miR-451a expression in RASF miR-451a compared to the control group RA SF (P < 0.0001) (Fig. 4d), accompanied by a significant reduction in *ATF2* expression (P < 0.001) (Fig. 4e). Additionally, there was a decrease in the expression of ATF2 protein in RASF miR-

 $^{451a}$  (P<0.01) (Fig. 4f). These findings indicate that miR-451a can negatively regulate the mRNA expression level of ATF2 in RA SF.

CCK-8 assay was used to assess the proliferation of RASF<sup>miR-451a</sup>, revealing that RASF<sup>miR-451a</sup> had a lower proliferation rate compared to RASF<sup>NC</sup> and control group RA SF (P < 0.0001) (Fig. 4g). The migration ability of rasfmiR-451a was assessed using a cell scratch assay, which showed that the scratch healing was slower in the RASF<sup>miR-451a</sup>. And the migration value was significantly reduced in the RASF<sup>miR-451a</sup> (P < 0.0001) (Fig. 4h). The invasion of RASF<sup>miR-451a</sup> was analyzed using a tranwell assay, which demonstrated that the number of cells that penetrated the tranwell chamber membrane was significantly lower in RASF<sup>miR-451a</sup> compared to the control group (P < 0.0001) (Fig. 4i). These results indicate that miR-451a may inhibit the proliferation, migration, and invasion of RASF.

## 3.3. Effect of hUCMSC-Exos<sup>miR-451a</sup> on RA SFs

The expression level of miR-451a was significantly increased in the RA SFs of Exos<sup>miR-451a</sup> group (P < 0.0001) (Fig. 4j), while the expression of ATF2 was significantly decreased (P < 0.001) (Fig. 4k). In the Exos group, miR-451a expression was increased, but it was lower than that of the Exos<sup>miR-451a</sup> group (P < 0.0001) (Fig. 4i). Additionally, there was a decrease in the expression of ATF2 protein in Exos<sup>miR-451a</sup> group (P <0.001), and lower than that in Exos group (P < 0.05) (Fig. 41). These results suggest that hUCMSC-Exos<sup>miR-451a</sup> may regulate the level of ATF2 by upregulating the level of miR-451a in RA SF. Compared to the control group, both 150 µg/mL hUCMSC-Exos<sup>miR-451a</sup> and hUCMSC-Exos were able to inhibit proliferation (P < 0.0001, P < 0.0001) (Fig. 4m), migration (P < 0.05, P < 0.001) (Fig. 4n), and invasion (P < 0.0001, P < 0.00010.0001) of RA SFs (Fig. 4-o). However, 150  $\mu g/mL~hUCMSC\text{-}Exos^{miR\text{-}451a}$ showed the most significant inhibitory effect on proliferation (P < 0.05) (Fig. 4m), migration (P < 0.05) (Fig. 4n), and invasion (P < 0.0001) (o) of RA SFs than hUCMSC-Exos. These findings suggest that hUCMSC-Exos<sup>miR-451a</sup> may regulate the mRNA level of ATF2 by upregulating the level of miR-451a in RA SFs, thereby inhibiting the proliferation, migration, and invasion of RA SFs.

## 3.4. Effect of hUCMSC-Exos<sup>miR-451a</sup> on CIA rats

Rats weighing 180-200 g were selected for the experiment to undergo two immune modeling processes and receive two treatments. On the 45th day, the required samples were collected. (Fig. 5a) After the initial immunization, the CIA rats exhibited a significant increase in the systemic performance score, which was characterized by the presence of single or two ear nodules and redness, as well as swelling of nasal hoof tissue, nodules at the tail, and swelling of front and rear toes. The systemic performance of CIA rats worsened after the second immunization. However, following the two interventions, the total score of systemic performance in the hUCMSC-Exos<sup>miR-451a</sup> intervention group and hUCMSC-Exos intervention group gradually decreased (Fig. Notably, the swelling of the front and rear toes showed improvement, while the other symptoms were slightly alleviated. Compared to the normal control group, the rate of weight growth in each group of rats slowed down after the primary immunization. After the secondary immunization, the rats in each group exhibited different changes in weight (Fig. 5c). However, there was no significant difference in weight among the groups at 45 days (P > 0.05) (Fig. 5d). One week after the initial immunization, the arthritis index of rats significantly increased. Rats with an arthritis index greater than 6 points were selected for the experiment. With re-immunization, the arthritis index continued to increase, but the rate of increase decreased compared to the previous round. Following the intervention, the arthritis index gradually decreased (Fig. 5e). The arthritis index of rats in the CIA model group at 45 days remained high, indicating a significant difference compared to the normal control group (p < 0.0001). However, the arthritis index decreased in both the hUCMSC-Exos  $^{miR\text{-}451a}$  group and the hUCMSCs-

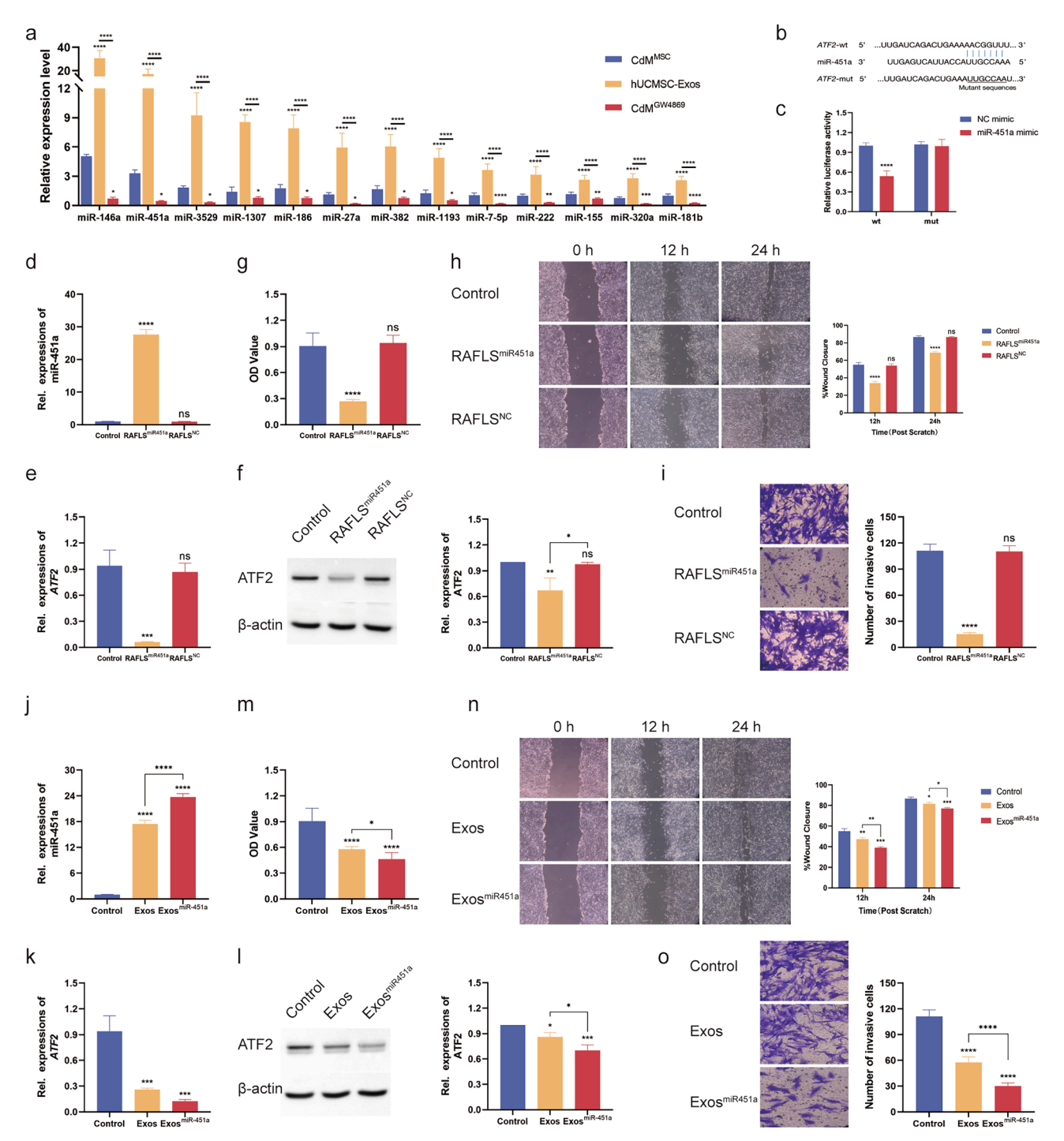


Fig. 4. The regulatory role of hUCMSC-Exos in the transfer of miRNAs between hUCMSCs and RA SFs (a) RT-qPCR confirmed the miRNAs that were upregulated in RA SFs after intervention with hUCMSC-Exos, which intersected with the miRNAs in hUCMSC-Exos. (b) The predicted binding site of miR-451a within the 3'-UTR of ATF2. The mutated binding site is also shown. (c) RA SFs were transfected with ATF2-wt or ATF2-mut in combination with miR-451a mimic or NC mimic; 48 h later, the luciferase activity was quantified. (d) RT-qPCR determined that the expression of miR-451a in RA SFs<sup>miR-451a</sup> was significantly upregulated. (e) RT-qPCR determined that the expression of ATF2 in RA SFs<sup>miR-451a</sup> was significantly reduced. (f) Western blot analysis determined that the expression of ATF2 protein in RA SFs<sup>miR-451a</sup>. (g) The CCK-8 assay revealed a reduced proliferative capacity of RA SF<sup>miR-451a</sup>. (h) The cell scratch assay showed reduced migration of RA SFs<sup>miR-451a</sup>. (i) The invasive ability of RA SFs<sup>miR-451a</sup> was decreased by Tranwell method. (j) RT-qPCR determined that the expression of miR-451a upregulated in RA SFs after the intervention of Exos<sup>miR-451a</sup>. (k) RT-qPCR determined that the expression of ATF2 protein in RA SFs after the intervention of Exos<sup>miR-451a</sup>. (n) The CCK-8 assay revealed a reduced reduced migration of RA SFs after the intervention of Exos<sup>miR-451a</sup>. (o) The invasive ability of RA SFs after the intervention of Exos<sup>miR-451a</sup>. (n) The cell scratch assay showed reduced migration of RA SFs after the intervention of Exos<sup>miR-451a</sup>. (o) The invasive ability of RA SFs after the intervention of Exos<sup>miR-451a</sup> were decreased by Tranwell method. \* p < 0.001, \*\*\* p < 0.001, \*\*\* p < 0.001, \*\*\* p < 0.001.

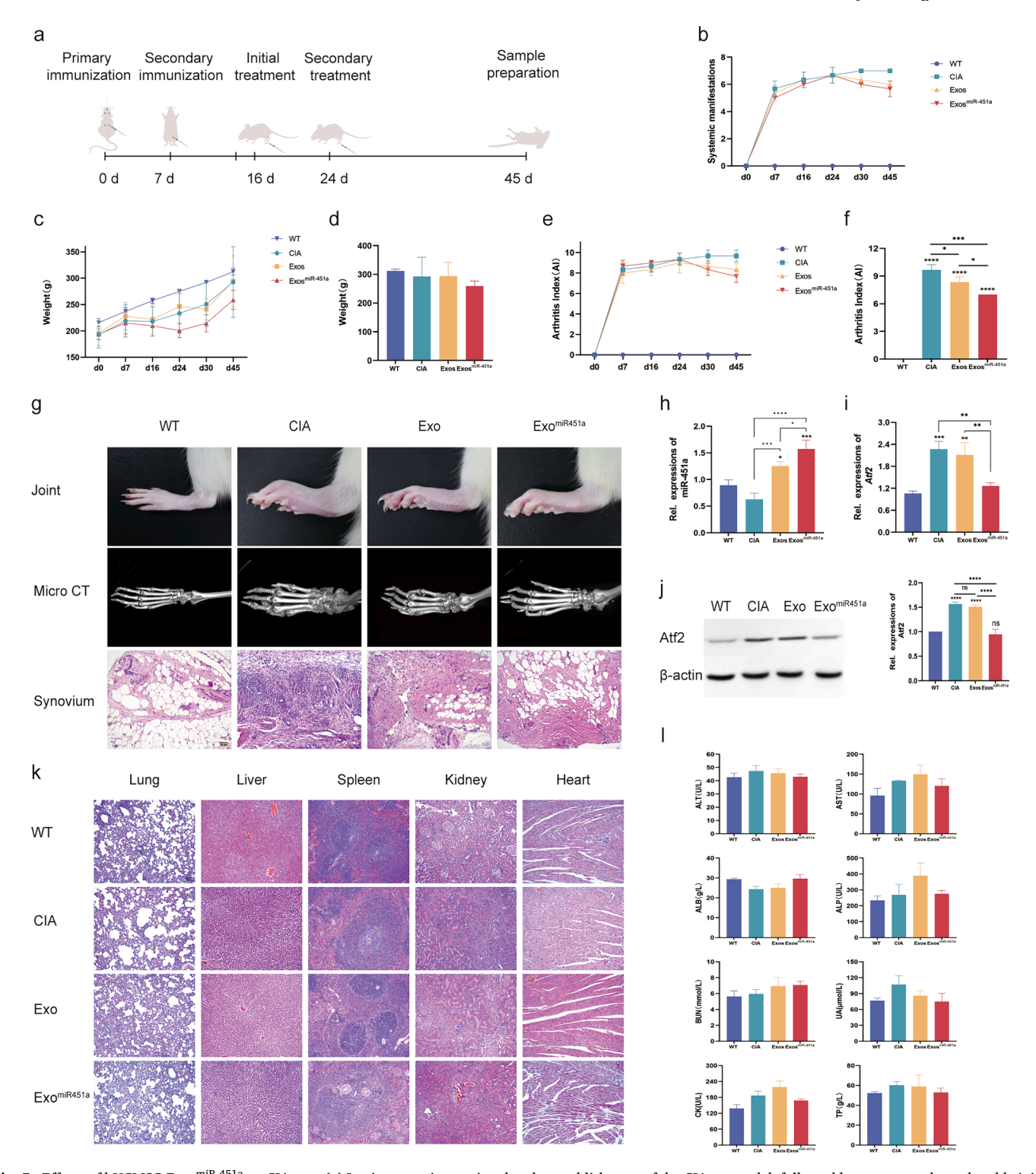


Fig. 5. Effects of hUCMSC-Exos<sup>miR-451a</sup> on CIA rats. (a) In vivo experiments involve the establishment of the CIA rat model, followed by treatment through ankle joint cavity injections, and finally, samples are collected for analysis. (b) Changes in systemic performance of rats during the experiment. (c) Changes in weight of each rat group during the experimental process. (d) On day 45, no significant weight differences were observed among the rat groups. (e) Changes in arthritis index of rats during the experiment. (f) On day 45, the arthritis index in the CIA rats remained high. The arthritis index for the hUCMSC-Exos<sup>miR-451a</sup> group was lower compared to the hUCMSC-Exos group. (g) On day 45, the CIA rats displayed severe cartilage and bone degradation. After receiving injections of hUCMSC-Exos<sup>miR-451a</sup> or hUCMSC-Exos, the bone destruction in the CIA rats was mitigated to a certain extent. The CIA rats exhibited severe synovitis. After receiving injections of hUCMSC-Exos<sup>miR-451a</sup> or hUCMSC-Exos, the synovitis in the CIA rats was alleviated. (h)(i)(j) Expression of miR-451a, ATF2 and ATF2 in the synovial tissue of different rat groups. In CIA rats treated with hUCMSC-Exos<sup>miR-451a</sup>, miR-451a expression increased, leading to the downregulation of ATF2. (k)(l) hUCMSC-Exos<sup>miR-451a</sup> or hUCMSC-Exos had good biosafety in CIA rats. No significant differences were observed in organ histopathology and biochemical indicators. \* P < 0.05, \*\* P < 0.01, \*\*\* P < 0.001, \*\*\* P < 0.001.

Exos group (p < 0.05, p < 0.01), with the arthritis index of the hUCMSC-Exos  $^{miR-451a}$  group being lower than that of the hUCMSCs-Exos group (p < 0.0001) (Fig. 5f).

On the 45th day, severe cartilage and bone destruction were observed in the CIA rats. The bone hollowing observed on the micro-CT image indicates the extent of severe bone damage (Fig. 5g). However, the treatment with hUCMSC-Exos miR-451a, hUCMSC-Exos alleviated the degree of bone destruction in CIA rats. Specifically, the bone loss in the ankle joint was milder in the treated mice compared to the control mice. These findings demonstrated that the use of hUCMSC-Exos and hUCMSC-Exos miR-451a had a positive effect on improving the bone destruction caused by collagen-induced arthritis.

Compared with the normal control group, the CIA model group exhibited obvious lesion degrees in the synovial tissue, characterized by a large number of inflammatory cell infiltrations and even the formation of panis around the synovium. However, after the injection of hUCMSC-Exos miR-451a and hUCMSC-Exos, the inflammatory cell infiltration in the synovial tissue of CIA rats decreased (Fig. 5g). The expression of miR-451a in the synovial tissue of CIA rats after the injection of hUCMSC-Exos miR-451a and hUCMSC-Exos was increased (P < 0.05, P < 0.001) (Fig. 5h). Additionally, Atf2 and Atf2 in the synovial tissue of CIA rats was downregulated in the hUCMSC-Exos miR-451a group (Fig. 5i)(Fig. 5j). No significant changes in organ pathology (Fig. 5k), biochemical indexes (Fig. 5l), and healthy rats were observed after injecting hUCMSC-Exos miR-451a and hUCMSC-Exos, suggesting their better biosafety.

### 4. Discussion

This study primarily focused on assessing the effectiveness of hUCMSC-Exos in treating RA. It is believed that hUCMSC-Exos modify the biological characteristics of RA SF by transmitting miR-451a, which further validates its efficacy in CIA rats.

Synovial fibroblasts (SFs) play a core role in the erosion and destruction of cartilage and bone tissue in RA joints. They are an important component of the synovial membrane. SFs exhibit characteristics such as excessive proliferation, invasion, and migration. They also have enhanced ability to secrete inflammatory factors and inhibit apoptosis. The pro-inflammatory phenotype of SFs is maintained by multiple surface molecules on their membrane in RA [10]. The cultured RA SFs expresses PDPN and CDH-11, with PDPN being linked to invasive cell growth and inflammatory factor secretion [11]. CDH-11, on the other hand, plays a role in regulating SF inflammatory response, promoting SF migration, and contributing to cartilage erosion [12].

Epigenetic modification in RA SFs plays a crucial role in the development and progression of RA. miRNAs, which are non-coding RNAs, are involved in post-transcriptional gene regulation. Abnormalities in the expression profile of miRNAs have been observed in RA patients. These dysregulated miRNAs participate in the pathogenesis of RA by regulating mRNA translation, inhibiting protein expression, and influencing various cellular processes. In RA SFs, the expression of miR-106b, miR-143, miR-145, miR-203, miR-221, and miR-483-3p is upregulated. Specifically, miR-106b is highly expressed not only in RA SFs but also in their derived Exos. Exos derived from RA SFs can deliver miR-106b to chondrocytes, where it targets PDK4, resulting in the inhibition of chondrocyte proliferation, migration, and acceleration of chondrocyte apoptosis [13]. MiR-143 and miR-145 target insulin-like growth factor binding protein 5 (IGFBP5) and signaling protein 3A (SEMA3A), respectively, in RA SFs, thereby affecting the biological function of these cells [14]. On the other hand, miR-203 is overexpressed in RA SF due to DNA methylation control, leading to increased expression of MMPs and IL-6 [15]. The expression of miR-221 is also upregulated in RA SFs, and its secretion is associated with the release of inflammatory factors such as TNF- $\alpha$ , IL-6, and IL-1 $\beta$ . Knocking down miR-221 in RA SFs results in decreased migration and invasion abilities [16,17]. In an inflammatorystimulated RA model, miR-221-3p expression was found to be upregulated in SFs, potentially targeting the Wnt and BMP signaling pathways,

thereby influencing bone loss [18] and compensatory bone formation [19]. Furthermore, upregulation of miR-483-3p promotes cell proliferation and inhibits apoptosis by targeting IGF-1. Exos derived from inflammatory-induced RA SFs contain differentially expressed miRNAs, such as miR-1307-3p targeting NDRG and inhibiting osteoclast-related gene expression [20], and miR-323a-5p targeting CD6 to weaken T cell activation signals [21]. On the other hand, some miRNAs are downregulated in RA SFs, impacting their biological characteristics. For instance, miR-23b inhibition by the NF-κB signaling pathway regulates joint inflammation [22]. Downregulation of miR-27a-3p expression promotes an increased apoptosis rate, inhibits cell proliferation, and reduces the secretion of IL-1 $\beta$ , IL-6, and TNF- $\alpha$  in RA SFs [23]. Similarly, downregulation of miR-29a in RA SFs inhibits their proliferation and induces apoptosis by targeting signal transduction and transcription activator 3 (STAT3), thereby suppressing the expression of inflammatory cytokines [24]. Additionally, decreased expression of miR-29c-3p upregulates COL1A1 and reduces FOXO1, thus promoting the proliferation, migration, and invasion of RA SFs [25].

The expression of miR-34a-5p in RA SFs is relatively low. Upregulation of miR-34a-5p directly targets X-box binding protein 1 (XBP1) [26] and inhibits the proliferation of SFs [27]. It also inhibits the secretion of TNF- $\alpha$  and IL-6 in SFs. Conversely, miR-137 is down-regulated in RA SFs and negatively correlated with inflammatory factors [28]. When miR-137 is upregulated, it inhibits the growth, migration, and invasion of HSF-RA. Additionally, it promotes cell apoptosis. In patients with rheumatoid arthritis, the levels of miR-150-5p in serum, synovial tissue, and SFs are significantly reduced [29]. Simultaneously, the levels of MMP14 and VEGF are increased. Its expression is associated with the activation state of RA SFs and inhibits the migration of RA SFs. On the other hand, miR-199a-3p [30], miR-449 [31], and miR-431-5p [32] are downregulated in RA SFs. These miRNAs promote cell proliferation and inhibit cell apoptosis by targeting RB1, HDAC1, and XIAP, respectively.

Taken together, these findings suggest that there is a miRNA imbalance in RA patients. Correcting these miRNA imbalances through exogenous miRNA intervention or regulation of endogenous miRNA expression may restore the biological dysfunction of RA SFs.

MSCs have immunomodulatory and differentiation effects. [33] At present research has proven the role of MSCs in various diseases and has therapeutic potential [34]. However MSCs may lead to abnormal differentiation tumor formation and induce anti donor immune responses. [35] One of the mechanisms of action of MSCs is their secretion of paracrine factors in the form of extracellular vesicles (EVs) in the tissue microenvironment. Exos is the smallest extracellular vesicle derived from MSC with low immunogenicity [36]. Exos is more effective less toxic and more stable than parental cells. Exos transfers various nucleic acids proteins and lipids from mother cells to receptor cells thereby participating in chronic inflammation and immune processes. At present MSC-Exo has become a new research hotspot in the medical field. Among them miRNAs have high abundance inherent stability and ease of sampling. The role of Exos miRNA has received widespread attention [37].

Exos, which promote direct intracellular transfer of miRNA between cells, have the potential to be a therapeutic strategy for RA. In vitro experiments have demonstrated effective transfection of miR-150-5p into BM-MSCs and subsequent delivery to RA SFs through EVs. By targeting MMP14 and VEGF, miR-150-5p was able to reverse proinflammatory factor-induced migration and invasion of RA SF, as well as downregulate tube formation in HUVEC. Furthermore, in vivo experiments using BM-MSCs-EV demonstrated that miR-150-5p can reduce posterior paw thickness and clinical arthritis scores in CIA mice [24] Overexpressing miRNA-124a in MSC-EV led to the inhibition of proliferation and migration of MH7A [38]. Additionally, it was observed that this overexpression also promoted apoptosis in these cells. Moreover, the use of miR-320a mimic, which targets CXCL9a in MSC-EV, was found to significantly inhibit the activation, migration, and invasion of

RA SFs [39], while also alleviating miR-34a in CIA. Furthermore, the study revealed that miR-34a can inhibit proliferation and activity of RA SF by inhibiting cyclin I and activating the ATM/ATR/p53 signaling pathway, ultimately inducing apoptosis in RA SFs [40]. Another interesting finding was that miR-205-5p present in BMSC-EV targets MDM2, leading to the inhibition of IL-1  $\beta$ -induced inflammation and inflammatory response in RA SFs of CIA mice [41]. Moreover, it was observed that miR-140-3p in HUCMSCs EV inhibits proliferation of RA SFs and promotes their apoptosis by downregulating serum- and glucose-dependent kinase 1 (SGK1), thus alleviating joint injury in RA rats [42].

This study identified 13 differential miRNAs that were upregulated in RA SFs following intervention with hUCMSC-Exos. These miRNAs were found to be enriched in hUCMSC-Exos, suggesting their potential involvement in the delivery of hUCMSC-Exos to RA SFs. Among these miRNAs, miR-146a exhibited the most pronounced changes. MiR-146a is a crucial epigenetic regulator of the innate immune response and its reduced expression in RA SFs leads to dysregulation of tumor necrosis factor (TNF) receptor correlated factor 6 (TRAF6), increased proliferation of RA SFs, and consequent joint destruction in TNF-driven arthritis models. Furthermore, the depletion of miR-146a enhances the ability of RA SFs to support osteoclastogenesis by influencing the balance between RANKL and osteoprotegerin (OPG), [43] both of which are key regulators of bone destruction. MiR-146a also targets the transcription factor STAT1, which is involved in interferon-gamma (IFN-γ) signaling and improves the inhibitory pathway of regulatory T cells (Treg cells).By downregulating STAT1 and limiting inflammation, miR-146a plays a crucial role in reducing pathogenic IFN-γ-mediated Th1 responses. [44] Moreover, MSC-derived Exos transduced with miR-146a significantly increase the expression of Treg cells in CIA mice, promoting an antiinflammatory response by enhancing the secretion of IL-10 and TGF-β. [45] Additionally, miR-146a-transduced MSC-derived Exos lead to a notable reduction in IFNy mRNA expression levels in CIA mice. [46]In conclusion, the significance of miR-146a in the context of RA has been widely recognized and investigated.

This study primarily investigated miR-451a, the second-most abundant microRNA after miR-146a. MiR-146a is known to be upregulated in RA SFs following hUCMSC-Exos intervention and is highly enriched in hUCMSC-Exos. However, the detailed exploration of miR-451a in the context of RA remains limited.

MiR-451a is associated with cell proliferation and migration, and is considered a tumor suppressor. miR-451a can reduce the invasiveness of colorectal cancer cells [47], inhibiting the proliferation and migration of glioma cells by targeting CAB39 and downregulating LKB1/AMPK signal transduction [48]. miR-451a exerts anti-tumor effects in melanoma by delaying cell migration and invasion. To verify whether miR-451a affects the biological characteristics of RA SF, a RA SFs model with miR-451a overexpression was constructed. It was found that miR-451a overexpression can inhibit the proliferation, migration, and invasion of RA SFs.

MiR-451a has been detected as the most enriched miRNA in many EVs of different cell types [49]. TargetScan predicted that miR-451a targets and regulates AFT2, a transcription factor belonging to the DNA binding protein leucine zipper family. The aberrant activation of ATF2 facilitates the proliferation and migration of invasive cancer cells [50,51]. ATF2 participates in the process of RA chronic inflammation [52]. Upregulation of ATF2 expression and phosphorylation in RA synovial tissue promotes the migration and invasion of RA SF [53]. Binding of miR-451 to 3 '- UTR of ATF2 transcript to promote its degradation [54]. Using a dual luciferase gene reporting system, we verified the regulatory relationship between miR-451a and ATF2. With RT qPCR, we found that overexpression of miR-451a in RA SFs had a significant downregulating effect on the mRNA level of ATF2. This confirmed the negative regulation of ATF2 expression by miR-451a in RA SFs, thereby impacting the proliferation, migration, and invasion of RA SFs.

Exos, as natural nanocarriers, have the potential to be used as

therapeutic agents for various diseases. Specifically, adipose stem cell Exos (ADSC-Exos) loaded with gold nanoparticles (GNPs) hydrogel can regulate macrophage immunity by delivering miR-451a. This regulation of macrophage immunity then effectively modulates bone immune metabolism, ultimately promoting bone tissue healing [55]. Furthermore, Exos<sup>miR-451a</sup> has demonstrated its role as a tumor suppressor within hepatocellular carcinoma (HCC) cell lines and human umbilical vein endothelial cells. It induces apoptosis in these cell lines and inhibits human umbilical vein endothelial cell migration, tube formation, and vascular permeability [56]. Additionally, miR-451a, when loaded in Exos derived from hUCMSCs, can also limit the epithelial-mesenchymal transformation of HCC cells by targeting lyagin metalloproteinase 10 [57].

In our study, we found that Exos loaded with miR-451a could effectively inhibit the proliferation, migration, and invasion of RA SFs by targeting ATF2. Notably, the inhibitory effect of miR-451a-loaded Exos was found to be stronger than that of natural Exos. Moreover, in CIA rats, Exos loaded with miR-451a improved joint inflammation by targeting synovial tissue Atf2, resulting in alleviation of joint pathological synovitis and improved imaging findings. Importantly, Exos loaded with miR-451a demonstrated good biosecurity.

### 5. Conclusion

This study reveals several significant findings. Firstly, hUCMSC-Exos were found to inhibit the proliferation, migration, and invasion of RA SFs. This effect was achieved by transmitting miR-451a, which targeted ATF2 and regulated its expression. Additionally, in a rat model, hUCMSC-Exos were proven to improve joint inflammation and alleviate joint pathological synovitis, as well as imaging manifestations. It is worth noting that engineered Exos not only maintained their innate immunomodulatory components but also reprogrammed the synovial microenvironment. Altogether, these results strongly support the targeted anti-inflammatory therapeutic effects of engineered Exos. Furthermore, this study offers unique insights into the treatment of RA and presents an effective strategy with broad prospects for future biomedical applications and clinical translation.

## **Funding**

This work was supported by grants from the National Natural Science Foundation of China (81871292), the Key Research and Development (R&D) Projects of Shanxi Province (201803D31136), Four "batches" innovation project of invigorating medical through science and technology of shanxi province(2023XM002), Shanxi Province Postgraduate Practice Innovation Project (2023SJ135) and Shanxi Province Postgraduate Innovation Project (2020BY080).

## CRediT authorship contribution statement

Liangyu Mi: Methodology, Resources, Software, Visualization, Writing – original draft. Jinfang Gao: Methodology, Visualization. Na Li: Methodology, Software. Ying Liu: Conceptualization. Na Zhang: Methodology, Software. Yanan Gao: Data curation, Visualization. Xinyue Peng: Data curation, Methodology. Liyun Zhang: Supervision. Ke Xu: Supervision, , Validation, Writing – review & editing.

#### Data availability

Our high-throughput sequencing data can be downloaded from NCBI GEO database under the accession numbers GSE237991 (https://www.ncbi.nlm.nih.gov/geo/query/acc.cgi?acc=GSE237991).

#### References

- [1] T. Németh, G. Nagy, T. Pap, Synovial Fibroblasts as Potential Drug Targets in Rheumatoid Arthritis, Where Do We Stand and Where Shall We Go? Ann. Rheum. Dis. 81 (2022) 1055–1064, https://doi.org/10.1136/annrheumdis-2021-222021.
- [2] F. Mirza, J. Lorenzo, H. Drissi, F.Y. Lee, D.Y. Soung, Dried Plum Alleviates Symptoms of Inflammatory Arthritis in TNF Transgenic Mice, J. Nutr. Biochem. 52 (2018) 54–61, https://doi.org/10.1016/j.jnutbio.2017.10.002.
- [3] M. Andersen, M. Boesen, K. Ellegaard, R. Christensen, K. Söderström, N. Søe, P. Spee, U.G. Mørch, S. Torp-Pedersen, E.M. Bartels, et al., Synovial Explant Inflammatory Mediator Production Corresponds to Rheumatoid Arthritis Imaging Hallmarks: A Cross-Sectional Study, Arthritis Res. Ther. 16 (2014) R107, https://doi.org/10.1186/ar4557.
- [4] C. Li, L. Lin, L. Zhang, R. Xu, X. Chen, J. Ji, Y. Li, Long Noncoding RNA P21 Enhances Autophagy to Alleviate Endothelial Progenitor Cells Damage and Promote Endothelial Repair in Hypertension through SESN2/AMPK/TSC2 Pathway, Pharmacol. Res. 173 (2021), 105920, https://doi.org/10.1016/j. phrs.2021.105920.
- [5] D.G. Phinney, M. Di Giuseppe, J. Njah, E. Sala, S. Shiva, C.M. St Croix, D.B. Stolz, S. C. Watkins, Y.P. Di, G.D. Leikauf, et al., Mesenchymal Stem Cells Use Extracellular Vesicles to Outsource Mitophagy and Shuttle microRNAs, Nat. Commun. 6 (2015) 8472, https://doi.org/10.1038/ncomms9472.
- [6] S.C. Abreu, D.J. Weiss, P.R.M. Rocco, Extracellular Vesicles Derived from Mesenchymal Stromal Cells: A Therapeutic Option in Respiratory Diseases? Stem Cell Res. Ther. 7 (2016) 53, https://doi.org/10.1186/s13287-016-0317-0.
- [7] J. Fafián-Labora, I. Lesende-Rodriguez, P. Fernández-Pernas, S. Sangiao-Alvarellos, L. Monserrat, O.J. Arntz, F.J. van de Loo, J. Mateos, M.C. Arufe, Effect of Age on Pro-Inflammatory miRNAs Contained in Mesenchymal Stem Cell-Derived Extracellular Vesicles, Sci. Rep. 7 (2017) 43923, https://doi.org/10.1038/ sren43923.
- [8] G. Meister, M. Landthaler, Y. Dorsett, T. Tuschl, Sequence-Specific Inhibition of microRNA- and siRNA-Induced RNA Silencing, RNA 10 (2004) 544–550, https://doi.org/10.1261/rna.5235104.
- [9] Y. Zhang, M. Zeng, B. Li, B. Zhang, B. Cao, Y. Wu, S. Ye, R. Xu, X. Zheng, W. Feng, Ephedra Herb Extract Ameliorates Adriamycin-Induced Nephrotic Syndrome in Rats via the CAMKK2/AMPK/mTOR Signaling Pathway, Chin. J. Nat. Med. 21 (2023) 371–382, https://doi.org/10.1016/S1875-5364(23)60454-6.
- [10] Z. Wu, D. Ma, H. Yang, J. Gao, G. Zhang, K. Xu, L. Zhang, Fibroblast-like Synoviocytes in Rheumatoid Arthritis: Surface Markers and Phenotypes, Int. Immunopharmacol. 93 (2021), 107392, https://doi.org/10.1016/j. intimp.2021.107392.
- [11] L.-Y. Mi, J.-F. Gao, D. Ma, L.-Y. Zhang, G.-L. Zhang, K. Xu, Application of Single-Cell Sequencing in Autoimmune Diseases, Chin Med. J. (Engl.) 134 (2020) 495–497, https://doi.org/10.1097/CM9.000000000001050.
- [12] E.H. Noss, G.F.M. Watts, D. Zocco, T.L. Keller, M. Whitman, C.P. Blobel, D.M. Lee, M.B. Brenner, Evidence for Cadherin-11 Cleavage in the Synovium and Partial Characterization of Its Mechanism, Arthritis Res. Ther. 17 (2015) 126, https://doi. org/10.1186/s13075-015-0647-9.
- [13] D. Liu, Y. Fang, Y. Rao, W. Tan, W. Zhou, X. Wu, C. Zhang, Y. Zhang, Y. Liu, M. Sunagawa, et al., Synovial Fibroblast-Derived Exosomal microRNA-106b Suppresses Chondrocyte Proliferation and Migration in Rheumatoid Arthritis via down-Regulation of PDK4, J. Mol. Med. (Berl) 98 (2020) 409–423, https://doi.org/10.1007/s00109-020-01882-2.
- [14] B.-K. Hong, S. You, S.-A. Yoo, D. Park, D. Hwang, C.-S. Cho, W.-U. Kim, MicroRNA-143 and -145 Modulate the Phenotype of Synovial Fibroblasts in Rheumatoid Arthritis, Exp. Mol. Med. 49 (2017) e363.
- [15] J. Stanczyk, C. Ospelt, E. Karouzakis, A. Filer, K. Raza, C. Kolling, R. Gay, C. D. Buckley, P.P. Tak, S. Gay, et al., Altered Expression of microRNA-203 in Rheumatoid Arthritis Synovial Fibroblasts and Its Role in Fibroblast Activation, Arthritis Rheum. 63 (2011) 373–381, https://doi.org/10.1002/art.30115.
- [16] S. Yang, Y. Yang, Downregulation of microRNA-221 Decreases Migration and Invasion in Fibroblast-like Synoviocytes in Rheumatoid Arthritis, Mol. Med. Rep. 12 (2015) 2395–2401, https://doi.org/10.3892/mmr.2015.3642.
- [17] I. Pandis, C. Ospelt, N. Karagianni, M.C. Denis, M. Reczko, C. Camps, A. G. Hatzigeorgiou, J. Ragoussis, S. Gay, G. Kollias, Identification of microRNA-221/222 and microRNA-323-3p Association with Rheumatoid Arthritis via Predictions Using the Human Tumour Necrosis Factor Transgenic Mouse Model, Ann. Rheum. Dis. 71 (2012) 1716–1723, https://doi.org/10.1136/annrheumdis-2011-200803.
- [18] Y. Maeda, N.H. Farina, M.M. Matzelle, P.J. Fanning, J.B. Lian, E.M. Gravallese, Synovium-Derived MicroRNAs Regulate Bone Pathways in Rheumatoid Arthritis, J. Bone Miner. Res. 32 (2017) 461–472, https://doi.org/10.1002/jbmr.3005.
- [19] L. Wang, Y. Yu, S. Ni, D. Li, J. Liu, D. Xie, H.Y. Chu, Q. Ren, C. Zhong, N. Zhang, et al., Therapeutic Aptamer Targeting Sclerostin Loop3 for Promoting Bone Formation without Increasing Cardiovascular Risk in Osteogenesis Imperfecta Mice, Theranostics 12 (2022) 5645–5674, https://doi.org/10.7150/thno.63177.
- [20] L. Li, H. Xu, L. Qu, M. Nisar, M. Farrukh Nisar, X. Liu, K. Xu, Water Extracts of Polygonum Multiflorum Thunb. and Its Active Component Emodin Relieves Osteoarthritis by Regulating Cholesterol Metabolism and Suppressing Chondrocyte Inflammation, Acupun. Herbal Med. 3 (2023) 96–106, https://doi.org/10.1097/ HM9.00000000000000061.
- [21] Y. Takamura, W. Aoki, A. Satomura, S. Shibasaki, M. Ueda, Small RNAs Detected in Exosomes Derived from the MH7A Synovial Fibroblast Cell Line with TNF- $\alpha$  Stimulation, PLoS One 13 (2018) e0201851.
- [22] S. Zhu, W. Pan, X. Song, Y. Liu, X. Shao, Y. Tang, D. Liang, D. He, H. Wang, W. Liu, et al., The microRNA miR-23b Suppresses IL-17-Associated Autoimmune

- Inflammation by Targeting TAB2, TAB3 and IKK- $\alpha$ , Nat. Med. 18 (2012) 1077–1086, https://doi.org/10.1038/nm.2815.
- [23] L. Chen, Q. Lu, J. Chen, R. Feng, C. Yang, Upregulating miR-27a-3p Inhibits Cell Proliferation and Inflammation of Rheumatoid Arthritis Synovial Fibroblasts through Targeting Toll-like Receptor 5, Exp. Ther. Med. 22 (2021) 1227, https://doi.org/10.3892/etm.2021.10661.
- [24] J. Liu, D. Fei, J. Xing, J. Du, MicroRNA-29a Inhibits Proliferation and Induces Apoptosis in Rheumatoid Arthritis Fibroblast-like Synoviocytes by Repressing STAT3, Biomed. Pharmacother. 96 (2017) 173–181, https://doi.org/10.1016/j. biopha.2017.09.120.
- [25] C.-C. Tseng, L.-Y. Wu, W.-C. Tsai, T.-T. Ou, C.-C. Wu, W.-Y. Sung, P.-L. Kuo, J.-H. Yen, Differential Expression Profiles of the Transcriptome and miRNA Interactome in Synovial Fibroblasts of Rheumatoid Arthritis Revealed by Next Generation Sequencing, Diagnostics (basel) 9 (2019) 98, https://doi.org/10.3390/diagnostics030098
- [26] X. Song, Q. Li, J. Zhang, A Double-Edged Sword: DLG5 in Diseases, Biomed. Pharmacother. 162 (2023), 114611, https://doi.org/10.1016/j. biopha.2023.114611.
- [27] A.-F. Song, L. Kang, Y.-F. Wang, M. Wang, MiR-34a-5p Inhibits Fibroblast-like Synoviocytes Proliferation via XBP1, Eur. Rev. Med. Pharmacol. Sci. 24 (2020) 11675–11682, https://doi.org/10.26355/eurrev\_202011\_23812.
- [28] W. Sun, Y. Zhang, G. Wang, MicroRNA-137-Mediated Inhibition of Lysine-Specific Demethylase-1 Prevents against Rheumatoid Arthritis in an Association with the REST/mTOR Axis, Mol. Pain 17 (2021), https://doi.org/10.1177/ 17449660211011847
- [29] Z. Chen, H. Wang, Y. Xia, F. Yan, Y. Lu, Therapeutic Potential of Mesenchymal Cell-Derived miRNA-150-5p-Expressing Exosomes in Rheumatoid Arthritis Mediated by the Modulation of MMP14 and VEGF, J. Immunol. 201 (2018) 2472–2482, https:// doi.org/10.4049/jimmunol.1800304.
- [30] Y. Wangyang, L. Yi, T. Wang, Y. Feng, G. Liu, D. Li, X. Zheng, MiR-199a-3p Inhibits Proliferation and Induces Apoptosis in Rheumatoid Arthritis Fibroblast-like Synoviocytes via Suppressing Retinoblastoma 1, Biosci. Rep. 38, BSR20180982 (2018), https://doi.org/10.1042/BSR20180982.
- [31] J. Guo, X. Cao, W. Zhao, H. Zhu, X. Ma, C. Hao, L. Wu, M. Zhang, Y. Yang, J. Zhao, et al., MicroRNA-449 Targets Histone Deacetylase 1 to Regulate the Proliferation, Invasion, and Apoptosis of Synovial Fibroblasts in Rheumatoid Arthritis, Ann. Palliat. Med. 10 (2021) 7960–7969, https://doi.org/10.21037/apm-21-1383.
- [32] Y. Wang, K. Zhang, X. Yuan, N. Xu, S. Zhao, L. Hou, L. Yang, N. Zhang, miR-431-5p Regulates Cell Proliferation and Apoptosis in Fibroblast-like Synoviocytes in Rheumatoid Arthritis by Targeting XIAP, Arthritis Res. Ther. 22 (2020) 231, https://doi.org/10.1186/s13075-020-02328-3.
- [33] Y. Zhu, R. Huang, Z. Wu, S. Song, L. Cheng, R. Zhu, Deep Learning-Based Predictive Identification of Neural Stem Cell Differentiation, Nat. Commun. 12 (2021) 2614, https://doi.org/10.1038/s41467-021-22758-0.
- [34] Y. Tang, S. Liu, Y. Deng, Y. Zhang, L. Yin, W. Zheng, An Improved Method for Soft Tissue Modeling, Biomed. Signal Process. Control 65 (2021), 102367, https://doi. org/10.1016/j.bspc.2020.102367.
- [35] H. Xu, K. Van Der Jeught, Z. Zhou, L. Zhang, T. Yu, Y. Sun, Y. Li, C. Wan, K.M. So, D. Liu, et al., Atractylenolide I Enhances Responsiveness to Immune Checkpoint Blockade Therapy by Activating Tumor Antigen Presentation, J. Clin. Investig. 131 (2021) e146832.
- [36] A. Gowen, F. Shahjin, S. Chand, K.E. Odegaard, S.V. Yelamanchili, Mesenchymal Stem Cell-Derived Extracellular Vesicles: Challenges in Clinical Applications, Front. Cell Dev. Biol. 8 (2020) 149, https://doi.org/10.3389/fcell.2020.00149.
- [37] X. Hu, S. Liao, H. Bai, L. Wu, M. Wang, Q. Wu, J. Zhou, L. Jiao, X. Chen, Y. Zhou, et al., Integrating Exosomal microRNAs and Electronic Health Data Improved Tuberculosis Diagnosis, EBioMedicine 40 (2019) 564–573, https://doi.org/10.1016/j.ebjom.2019.01.023.
- [38] H.-Y. Meng, L.-Q. Chen, L.-H. Chen, The Inhibition by Human MSCs-Derived miRNA-124a Overexpression Exosomes in the Proliferation and Migration of Rheumatoid Arthritis-Related Fibroblast-like Synoviocyte Cell, BMC Musculoskelet. Disord. 21 (2020) 150, https://doi.org/10.1186/s12891-020-3159-y.
- [39] Q. Meng, B. Qiu, Exosomal MicroRNA-320a Derived From Mesenchymal Stem Cells Regulates Rheumatoid Arthritis Fibroblast-Like Synoviocyte Activation by Suppressing CXCL9 Expression, Front. Physiol. 11 (2020) 441, https://doi.org/ 10.3389/fphys.2020.00441.
- [40] H. Wu, X. Zhou, X. Wang, W. Cheng, X. Hu, Y. Wang, B. Luo, W. Huang, J. Gu, miR-34a in Extracellular Vesicles from Bone Marrow Mesenchymal Stem Cells Reduces Rheumatoid Arthritis Inflammation via the Cyclin I/ATM/ATR/P53 Axis, J. Cell Mol. Med. 25 (2021) 1896–1910, https://doi.org/10.1111/jcmm.15857
- [41] W. Ma, F. Tang, L. Xiao, S. Han, X. Yao, Q. Zhang, J. Zhou, Y. Wang, J. Zhou, miR-205-5p in Exosomes Divided from Chondrogenic Mesenchymal Stem Cells Alleviated Rheumatoid Arthritis via Regulating MDM2 in Fibroblast-like Synoviocytes, J. Musculoskelet. Neuronal Interact. 22 (2022) 132–141.
- [42] Y. Huang, L. Chen, D. Chen, P. Fan, H. Yu, Exosomal microRNA-140-3p from Human Umbilical Cord Mesenchymal Stem Cells Attenuates Joint Injury of Rats with Rheumatoid Arthritis by Silencing SGK1, Mol. Med. 28 (2022) 36, https://doi. org/10.1186/s10020-022-00451-2.
- [43] V. Saferding, A. Puchner, E. Goncalves-Alves, M. Hofmann, M. Bonelli, J. S. Brunner, E. Sahin, B. Niederreiter, S. Hayer, H.P. Kiener, et al., MicroRNA-146a Governs Fibroblast Activation and Joint Pathology in Arthritis, J. Autoimmun. 82 (2017) 74–84, https://doi.org/10.1016/j.jaut.2017.05.006.
- [44] U. Testa, E. Pelosi, G. Castelli, C. Labbaye, miR-146 and miR-155: Two Key Modulators of Immune Response and Tumor Development, Noncoding RNA 3 (2017) 22, https://doi.org/10.3390/ncrna3030022.

- [45] F. Tavasolian, A.Z. Hosseini, S. Soudi, M. Naderi, miRNA-146a Improves Immunomodulatory Effects of MSC-Derived Exosomes in Rheumatoid Arthritis, Curr. Gene Ther. 20 (2020) 297–312, https://doi.org/10.2174/ 1566523220666200916120708.
- [46] Z. Ren, X. Liu, E. Abdollahi, F. Tavasolian, Genetically Engineered Exosomes as a Potential Regulator of Th1 Cells Response in Rheumatoid Arthritis, Biopreserv Biobank 21 (2023) 355–366, https://doi.org/10.1089/bio.2022.0003.
- [47] K. Xu, B. Han, Y. Bai, X.-Y. Ma, Z.-N. Ji, Y. Xiong, S.-K. Miao, Y.-Y. Zhang, L.-M. Zhou, MiR-451a Suppressing BAP31 Can Inhibit Proliferation and Increase Apoptosis through Inducing ER Stress in Colorectal Cancer, Cell Death Dis. 10 (2019) 152, https://doi.org/10.1038/s41419-019-1403-x.
- [48] R. Ruhl, S. Rana, K. Kelley, C. Espinosa-Diez, C. Hudson, C. Lanciault, C.R. Thomas, V. Liana Tsikitis, S. Anand, microRNA-451a Regulates Colorectal Cancer Proliferation in Response to Radiation, BMC Cancer 18 (2018) 517, https://doi. org/10.1186/s12885-018-4370-1.
- [49] J. Guduric-Fuchs, A. O'Connor, B. Camp, C.L. O'Neill, R.J. Medina, D.A. Simpson, Selective Extracellular Vesicle-Mediated Export of an Overlapping Set of microRNAs from Multiple Cell Types, BMC Genomics 13 (2012) 357, https://doi. org/10.1186/1471-2164-13-357.
- [50] A.J. Berger, H.M. Kluger, N. Li, E. Kielhorn, R. Halaban, Z. Ronai, D.L. Rimm, Subcellular Localization of Activating Transcription Factor 2 in Melanoma Specimens Predicts Patient Survival, Cancer Res. 63 (2003) 8103–8107.
- [51] M.A. Loeffler, J. Hu, M. Kirchner, X. Wei, Y. Xiao, T. Albrecht, C. De La Torre, C. Sticht, J.M. Banales, M.N. Vogel, et al., miRNA Profiling of Biliary Intraepithelial Neoplasia Reveals Stepwise Tumorigenesis in Distal Cholangiocarcinoma via the miR-451a/ATF2 Axis, J. Pathol. 252 (2020) 239–251, https://doi.org/10.1002/ path.5514.

- [52] B. Li, N. Li, L. Zhang, K. Li, Y. Xie, M. Xue, Z. Zheng, Hsa\_circ\_0001859 Regulates ATF2 Expression by Functioning as an MiR-204/211 Sponge in Human Rheumatoid Arthritis, J. Immunol. Res. 2018 (2018) 9412387, https://doi.org/ 10.1155/2018/9412387.
- [53] X. Zhang, D. Zhang, Q. Wang, X. Guo, J. Chen, J. Jiang, M. Li, W. Liu, Y. Gao, Q. Zhang, et al., Sprouty2 Inhibits Migration and Invasion of Fibroblast-Like Synoviocytes in Rheumatoid Arthritis by Down-Regulating ATF2 Expression and Phosphorylation, Inflammation 44 (2021) 91–103, https://doi.org/10.1007/s10753-020-01311-z.
- [54] G. Lv, Z. Hu, Y. Tie, J. Du, H. Fu, X. Gao, X. Zheng, MicroRNA-451 Regulates Activating Transcription Factor 2 Expression and Inhibits Liver Cancer Cell Migration, Oncol. Rep. 32 (2014) 1021–1028, https://doi.org/10.3892/ or.2014.3296.
- [55] R. Li, D. Li, H. Wang, K. Chen, S. Wang, J. Xu, P. Ji, Exosomes from Adipose-Derived Stem Cells Regulate MI/M2 Macrophage Phenotypic Polarization to Promote Bone Healing via miR-451a/MIF, Stem Cell Res. Ther. 13 (2022) 149, https://doi.org/10.1186/s13287-022-02823-1.
- [56] S. Zhao, J. Li, G. Zhang, Q. Wang, C. Wu, Q. Zhang, H. Wang, P. Sun, R. Xiang, S. Yang, Exosomal miR-451a Functions as a Tumor Suppressor in Hepatocellular Carcinoma by Targeting LPIN1, Cell. Physiol. Biochem. 53 (2019) 19–35, https://doi.org/10.33594/000000118.
- [57] Y. Xu, Y. Lai, L. Cao, Y. Li, G. Chen, L. Chen, H. Weng, T. Chen, L. Wang, Y. Ye, Human Umbilical Cord Mesenchymal Stem Cells-Derived Exosomal microRNA-451a Represses Epithelial-Mesenchymal Transition of Hepatocellular Carcinoma Cells by Inhibiting ADAM10, RNA Biol. 18 (2021) 1408–1423, https://doi.org/ 10.1080/15476286.2020.1851540.